

Partial-Wave Amplitudes and Resonances in $\bar{p} + p \rightarrow \pi + \pi$

B. R. Martin

*Department of Physics and Astronomy, University College London,
London WC1E 6BT, England*

G. C. Oades

*Institute of Physics and Astronomy, Aarhus University,
DK-8000 Aarhus C, Denmark*

(submitted to Phys. Rev. D)

Abstract

Partial wave amplitudes have been extracted from accurate data on $\bar{p}p \rightarrow \pi^- \pi^+$, combined with earlier data on $\bar{p}p \rightarrow \pi^0 \pi^0$, by a method which incorporates the theoretical constraints of analyticity and crossing symmetry. The resulting solution gives a good fit to the annihilation data and is also consistent with the wealth of information in the crossed channel $\pi N \rightarrow \pi N$. The partial wave amplitudes show evidence for resonances in all partial waves with $J \leq 5$, at least one of which, a $J = 0^+$ state, (and possibly another with $J = 1^-$) is unlikely to have a simple $q\bar{q}$ structure.

13.75.Cs, 11.80.Et, 14.40.Cs, 25.43.+t

I. INTRODUCTION

There have been a number of attempts to obtain information on meson resonances from data on the reaction $\bar{N}N \rightarrow \pi\pi$. Earlier work [1] was restricted to testing the compatibility of data with assumed combinations of Breit-Wigner resonances and smooth backgrounds. These analyses used data only on the channel $\pi^-\pi^+$ [2] and the results, in the main, are in strong disagreement with later $\pi^0\pi^0$ data [3]. An alternative approach is to use the Barrelet zero method [4] to translate the dips observed in the angular distributions (cross-sections and asymmetries) into complex zeros of the scattering amplitudes. This method requires a number of assumptions to obtain smooth zero trajectories and to fix the overall phase of the solution. The latter is crucial, because in the absence of an optical theorem the method only determines the moduli and *relative* phases of the amplitudes at each energy. One choice is to assume a Breit-Wigner form for a particular partial wave, but different choices of input phases, however plausible, lead to different solutions for the partial waves, as can be seen by comparing the results of references [5] and [6].

An alternative method of obtaining amplitudes which overcomes the objections to earlier work, is to exploit analyticity via dispersion relations and determine the overall phase by using crossing symmetry to relate the annihilation data to known $\pi N \rightarrow \pi N$ elastic scattering amplitudes. This in principle overcomes the problem of the absence of an optical theorem and ensures that the resulting amplitudes not only fit the annihilation data, but are also consistent with the wealth of information on the crossed channel, $\pi N \rightarrow \pi N$. Dispersion relations at fixed- t or fixed- u are unsuitable because of the need to have information in unphysical regions, but this can be avoided by writing dispersion relations along hyperbolae in the Mandelstam plane [7]. In a previous paper [8] we presented a largely model-independent set of invariant amplitudes, which by construction satisfy analyticity and crossing symmetry and simultaneously give an excellent fit to all $\bar{p}p \rightarrow \pi\pi$ data (both in charged and neutral channels) existing at the time [2,3,9] and to amplitudes for $\pi N \rightarrow \pi N$. Subsequently [10] we showed that the structure in the invariant amplitudes, which reflects that seen directly in

the experimental data, was due to the existence of resonances in the partial wave amplitudes and we presented evidence for resonance activity in four states with spins 1, 2, 3 and 4.

Since our earlier work, new differential cross-section and asymmetry data have been obtained on the $\pi^-\pi^+$ channel at 20 center-of-mass energies in the range 1.91 MeV to 2.27 MeV [11] using the LEAR facility at CERN. These data are consistent with the earlier data [2], but are more accurate and also extend asymmetry measurements to lower momenta than previous experiments. However, the new experiments cover a slightly smaller range of energy. Here we present an analysis of the new data, plus the older $\pi^0\pi^0$ data [3], using as constraints the invariant amplitudes obtained in [8], thus indirectly imposing analyticity and crossing symmetry on the solution. We compare our results with other recent analyses [12–14] at the end of this paper.

II. PARTIAL-WAVE AMPLITUDES

The analysis of [8] was performed in terms of the usual πN invariant amplitudes A and B . In the t -channel, $\bar{N}N \rightarrow \pi\pi$, it is more convenient to work with B and

$$C \equiv -A + M \left(\frac{q}{p} \right) \cos \theta_t B, \quad (1)$$

where $q(p)$ is the center-of-mass momentum in the $\pi\pi(\bar{N}N)$ channel; M is the nucleon mass; and θ_t is the scattering angle in the t -channel. In the helicity basis, these two invariant amplitudes may be expressed in terms of partial-wave amplitudes by the expansions

$$B^I(t, \cos \theta_t) = \frac{8\pi}{p} \sum_J \frac{2J+1}{\sqrt{J(J+1)}} P'_J(\cos \theta_t) F_J^I(t) \quad (2)$$

and

$$C^I(t, \cos \theta_t) = \frac{4\pi\sqrt{t}}{p} \sum_J (2J+1) P_J(\cos \theta_t) N_J^I(t). \quad (3)$$

In these relations, N_J^I and F_J^I are the partial-wave helicity amplitudes for definite t -channel isospin I corresponding to t -channel helicity non-flip and flip, respectively, and t is the square of the center-of-mass energy in the t -channel. By Bose statistics,

$$N_J^1(t) \equiv F_J^1(t) \equiv 0 \quad \text{for } J \text{ even} \quad (4)$$

and

$$N_J^0(t) \equiv F_J^0(t) \equiv 0 \quad \text{for } J \text{ odd.} \quad (5)$$

In addition, $F_0^0 \equiv 0$. The helicity amplitudes are normalized such that the integrated cross-section for $\overline{N}N \rightarrow \pi\pi$ for a definite isospin I is

$$\sigma^I = 2\pi \left(\frac{q}{p}\right) \sum_J (2J+1) \left\{ |N_J^I|^2 + |F_J^I|^2 \right\}. \quad (6)$$

An alternative, but equivalent, way of expressing the partial-wave content of the invariant amplitudes is to use the LS basis. If we label the new amplitudes by JL , i.e. H_{JL} , then, for a fixed value of isospin I , they are related to N_J and F_J by

$$H_{J,L=J-1} = \left(\frac{2}{2J+1}\right)^{1/2} \left\{ \sqrt{J+1}F_J - \sqrt{J}N_J \right\} \quad (7)$$

and

$$H_{J,L=J+1} = \left(\frac{2}{2J+1}\right)^{1/2} \left\{ \sqrt{J}F_J + \sqrt{J+1}N_J \right\} \quad (8)$$

with

$$\sigma = \pi \left(\frac{q}{p}\right) \sum_J (2J+1) \left\{ |H_{J+}|^2 + |H_{J-}|^2 \right\}, \quad (9)$$

where $H_{J\pm} \equiv H_{J,L=J\pm 1}$. We will use both sets of amplitudes in the following discussion.

In [8], the invariant amplitudes were obtained along families of hyperbolic curves in the Mandelstam plane defined by a parameter

$$\xi \equiv \frac{(M^2 - m^2)^2 - s(\Sigma - s - t)}{t - 4m^2} \quad (10)$$

where m is the pion mass; s is the square of the center-of-mass energy in the s -channel $\pi N \rightarrow \pi N$; and $\Sigma \equiv 2(M^2 + m^2)$. Values of ξ were chosen so that the hyperbolae covered the t -channel region being analysed while staying almost entirely within the physical s -channel. To obtain amplitudes at the experimental energies, those from ref. [8] were linearly interpolated in t along the hyperbolae at fixed- ξ .

III. FITS TO DATA AND AMPLITUDES

The data fitted consisted of experimental differential cross-sections and asymmetries for $\bar{p}p \rightarrow \pi^- \pi^+$ at 20 momenta in the range 360 MeV/c to 1550 MeV/c [11] and, at each momentum, the invariant amplitudes from ref. [8] at a grid of ξ -values (or equivalently, a grid of values of $\cos \theta_t$). In addition, differential cross-sections for $\bar{p}p \rightarrow \pi^0 \pi^0$ were included by interpolating the measured data of ref. [3] to the momenta of the charged channel data. At each momentum we minimized the sum of the values for χ^2 per data point for each type of data. The parameters are, at each t -value, the complex amplitudes N_J^I and F_J^I . The number of amplitudes used in the partial-wave expansions is dictated by the form of the invariant amplitudes and the need to ensure a good representation of them, and not by criteria such as polynomial fits to the measured angular distributions, which are often truncated where the highest partial wave is still quite large. This is an important difference between our method and others [5,6,12,13] which use observables in the form of Legendre series truncated at a point where the size of the highest coefficient is actually large. Our interpolation of the t -channel data used a method that makes no assumption about the number of partial waves which are important (see Appendix C of ref. [8]), although we would expect higher partial waves to be progressively less important at lower momenta.

At each t -value, sufficient terms were used to obtain a good fit to each amplitude and to ensure reasonable smoothness of the resulting helicity amplitudes from one t -value to the next. In practice, 4-5 J -values were used at the lowest momentum, rising to 6-7 at the highest. Initial estimates of N_J^I and F_J^I were obtained from [8] and used as starting values in a simultaneous fit to all the data at a given momentum. In Table I we show values of χ^2 per data point for the differential cross-sections and asymmetries in the charged channel and for the amplitudes at each of the twenty momenta. At the higher momenta we also show values of χ^2 per data point for the neutral data. In Figs 1 and 2 we show the fits and/or predictions for the $\pi^+ \pi^-$ and $\pi^0 \pi^0$ data at three representative momenta. To give some idea of the quality of the fits to the invariant amplitudes, we show in Fig. 3 the fits to the

real and imaginary parts of B^\pm and C^\pm as functions of t at a fixed value of the hyperbolic parameter, $\xi = -0.04572 \text{ GeV}^2$.

IV. RESONANCES

The extraction of “hard” information on resonances from partial-wave amplitudes is a notoriously difficult problem, which has not been solved in a rigorous way even for elastic two-body reactions, and ultimately one has to resort to plausible models. We will use criteria which have proved successful in analysing reactions such as $\pi N \rightarrow \pi N$. Thus, we will use combinations of Breit-Wigner resonances and flexible non-resonant backgrounds with initial parameters suggested by loops in Argand diagrams, enhancements in the integrated partial cross-sections, maxima in amplitude speed plots etc., not by fitting the original experimental data. Before doing that, however, it is useful to see to what extent the “continuity” of the partial-wave amplitudes, which were obtained by a series of fits at fixed values of the energy, is compatible with partial-wave analyticity. To test this we have fitted the “raw” amplitudes with the following parametric forms constructed by analogy with the work of ref. [8].

$$H_{J,L=J\pm 1} = (1 - z_+)^L (1 + z_-)^2 \left[\sum_{n=0}^{N_-} a_n z_-^n + \sum_{n=1}^{N_+} b_n z_+^n + \sum_{n=1}^{N_u} c_n z_u^n \right], \quad (11)$$

where the variables z_- , z_+ and z_u are given by

$$z_- = \frac{a_- - (t - t_L)^{1/2}}{a_- + (t - t_L)^{1/2}}, \quad (12)$$

$$z_+ = \frac{a_+ - (4 M^2 - t)^{1/2}}{a_+ + (4 M^2 - t)^{1/2}} \quad (13)$$

and

$$z_u = \frac{a_u - (4 m^2 - t)^{1/2}}{a_u + (4 m^2 - t)^{1/2}}. \quad (14)$$

Here we use the values $a_- = a_u = 1 \text{ GeV}$ and $a_+ = 2 \text{ GeV}$ for the mapping constants. In eq.12 t_L is given by

$$t_L = m^2 \left(4 - \frac{m^2}{M^2} \right). \quad (15)$$

The three terms in eq.11 ensure that $H_{J,L=J\pm 1}$ has the correct analyticity properties as a function of t . The factor $(1 - z_+)^L$ ensures the correct behaviour at the $\overline{N}N$ threshold while the factor $(1 + z_-)^2$ ensures a suitable high energy behaviour. We do not attempt to impose the correct behaviour at the $\pi\pi$ pseudo-threshold since this is very far away from the energy region in which we are interested. The advantage in using such an a representation in the JL basis is that the $\overline{N}N$ threshold behaviour can be easily imposed, whereas in the helicity basis this is more difficult since the threshold behaviours of the two helicity states are correlated. The price for this decoupling is a correlation between the two JL basis amplitudes at $t = 0$ to avoid a spurious singularity at this point. However, this is again so far from the energy region in which we are interested that we ignore this problem.

The coefficients a_n , b_n and c_n in eq.11 are determined by fitting the values of $H_{J,L=J\pm 1}$ at the different t -values using the Pietarinen technique as described in ref. [8]. In these fits we use $N_- = N_u = 10$ and $N_+ = 15$ and are able to achieve good fits; it should be remarked that in these fits we take no account of correlations, neither between different amplitudes nor between the real and imaginary parts in the same amplitude. The results of these fits are shown as the solid curves in Fig. 4 for $J \leq 5$ where we show the dimensionless amplitudes

$$h_{J\pm}(W) = (pq)^{1/2} H_{J,L=J\pm 1}(W). \quad (16)$$

The $J = 6$ amplitudes are small and featureless and so are not shown. We conclude that, in the main, the single-energy amplitudes are compatible with partial-wave analyticity within plausible errors. In what follows, we have used these smooth amplitudes as the starting point for our extraction of resonance information. This is done for convenience, and it is worth remarking that no extra structure is introduced by the smoothing procedure and that we have checked that our conclusions are unaltered when the “raw” amplitudes are fitted.

In Fig. 4 we also show the contributions of each partial-wave helicity amplitude to the integrated partial cross-section. Some systematic features are immediately apparent.

Firstly, in a given energy region odd- J contributions are larger than those with even- J . This is of course directly related to the experimental observation that the $\pi^0\pi^0$ cross-section is approximately 1/3 of the $\pi^-\pi^+$ cross-section over the whole of the energy range we consider. We also note the increasing importance of partial waves with lower L as the energy decreases. Many partial waves show counterclockwise loops, with the amplitude moving rapidly over some part of the energy range; the classic signal of resonance activity. To obtain resonance parameters, we have fitted the dimensionless amplitudes with the parametric forms

$$h_{J\pm}(W) = \frac{\alpha_{J\pm}}{M_R - W - i\Gamma/2} + \tilde{p}^{L+1/2} \sum_{n=1}^{n_{JL}} \beta_{J\pm}^{(n)} x^{n-1} \quad (17)$$

where $W \equiv \sqrt{t}$ and

$$x \equiv \frac{2W - W_{\min} - W_{\max}}{W_{\max} - W_{\min}}. \quad (18)$$

In the background term the coefficients $\beta_{J\pm}^{(n)}$ are complex parameters, and to ensure the correct behaviour at the $\bar{N}N$ threshold we set $\tilde{p} = p/p_B$ where p_B is a suitable momentum, in practice taken to correspond to $W = 2.1\text{GeV}$. In the resonance term, the parameters are the mass M_R , the width Γ and the complex residue $\alpha_{J\pm}$. To ensure the correct behaviour at the $\bar{N}N$ threshold, we set

$$\begin{aligned} \alpha_{J\pm} &= \gamma_{J\pm} \left(\frac{p}{p_R}\right)^{L+1/2}, & p \leq p_R \\ &= \gamma_{J\pm}, & p > p_R \end{aligned} \quad (19)$$

where p_R is the value of p at $W = M_R$ and $\gamma_{J\pm}$ is a complex constant. Both amplitudes for a given J were fitted simultaneously, and in the absence of a realistic error analysis equal weights were assigned to each point. The results obtained by fitting the amplitudes as functions of energy, and the associated Argand diagrams, are shown as dashed lines in Fig. 4 where it will be seen that the fits are as good as those using the more general parametrization of eq.11

The $J = 0$ amplitude shows a clear resonance loop corresponding to a mass of 1.95 GeV/ c^2 and a width 0.16 GeV. The resonance dominates the real part at low energies,

but there is a large background at the upper end of the range. The imaginary part has significant contributions from both resonance and background terms throughout the entire energy range. In the case of the $J = 1$ amplitudes, there is a clear resonance signal in the $L = 0$ amplitude corresponding to a mass of $1.97 \text{ GeV}/c^2$ and a width of 0.14 GeV . This is accompanied by a substantial background contribution. The $L = 2$ amplitude is by comparison much smaller. For $J = 2$, both h_{2-} and h_{2+} amplitudes have resonance behaviour. The mass is $1.93 \text{ GeV}/c^2$ and the width is 0.15 GeV . The $J = 3$ state has a resonance in the h_{3-} amplitude with a mass of $2.02 \text{ GeV}/c^2$ and a width of 0.22 GeV . The width in the case of the raw amplitudes is slightly larger at 0.26 GeV . The h_{3+} amplitude is very small. The resonance in the $J = 4$ wave, which again is more prominent in the $L = J - 1$ amplitude, has a mass of $2.02 \text{ GeV}/c^2$ and a width of 0.14 GeV , which rises to 0.26 GeV in the case of the raw amplitudes. The mass is in good agreement with that of the well-established $f_4(2050)$ resonance, and the values for the width span the accepted value of 0.21 GeV . The fact that this state emerges clearly from our analysis lends weight to the validity of our procedures and the parameters of the other predicted resonances. In the $J = 5$ wave there is evidence for a state at $2.19 \text{ GeV}/c^2$ with a width of 0.22 GeV , again coupling stronger to the $L = J - 1$ amplitude. Finally, there is some evidence for a broad resonance in $J = 6$, but as this is just outside the range of the analysis, and the raw amplitudes shown much more scatter, we do not comment on this possibility further and it is therefore not shown.

The resonance masses and widths are summarised in Table II. Where two values are given, the first corresponds to fitting the raw amplitudes and the second to fitting the smoothed amplitudes. In the other cases both values are the same. Table II also gives the values of the product of the branching ratios

$$B_J \equiv B(R \rightarrow \pi\pi)B(R \rightarrow \overline{N}N), \quad (20)$$

calculated from the values of the residue parameters $\gamma_{J\pm}$. The only case where there is a well-established resonance is the $J^P = 4^+$ state $f_4(2050)$ with a measured mass of 2.044 ± 0.011

GeV/c² and a width of 0.208 ± 0.013 GeV. If we identify our $J = 4$ state with this, we can use the known $\pi\pi$ branching ratio of the $f_4(2050)$ of 17% to estimate the $\bar{N}N$ branching ratio to be between 2% and 8%, which is not inconsistent with a conventional $\bar{q}q$ resonance. If we assume that $\pi\pi$ branching ratios in the range 10-20% are also typical of daughter states in this mass range, then we can see from Table II that the other predicted resonances with $J = 2, 3$ and 5 have $\bar{N}N$ branching ratios similar to that of the $f_4(2050)$. However, the states with $J = 0$ and 1 are different and have far larger branching ratios. Indeed for the $J = 0$ state the coupling is probably unreasonably large, but in this case there is a very large background accompanying the resonance and in this situation our simple parameterisation may not be appropriate to extract accurate resonance parameters. Such states are unlikely to be conventional $\bar{q}q$ mesons, but are more likely to have a multiquark $\bar{q}q\bar{q}q$ structure [15].

V. OTHER ANALYSES AND CONCLUSIONS

Three other analyses [12–14] of the accurate $\pi^-\pi^+$ data [11] have been published. In ref. [12] it is assumed from the outset that the data can be fitted by partial-wave amplitudes each of which is parameterised in terms of towers of nearly degenerate resonances. The analysis then fits all the data [2,3,11] simultaneously. The motivation for this assumption is based on qualitative features of the data, such as the persistence of a very large polarization over a wide energy range, but nevertheless is really only testing the compatibility of the data with an assumed parametric form, like analyses of earlier data [1]. The resulting speed plots show little evidence for resonance-like behaviour and only the $J = 4$ and 5 amplitudes show clear peaks. This illustrates the strong correlations that exist between the states in the various towers and makes it difficult to ascribe much reliability to the parameters of individual resonances. This is further illustrated by the predicted values of B_J which, with the sole exception of the $J = 4$ state, where the mass and width were fixed from experiment, all indicate very large branching ratios to the $\bar{N}N$ channel.

The analysis of ref. [13] is based on the Barrelet method [4] and therefore has the usual

problems intrinsic to that method associated with the unresolved phase. The initially very large number of possible solutions is reduced by using the $\pi^0\pi^0$ data [3] and further reduced by imposing threshold behaviour on the way zeros appear, leaving just two solutions (A and B), both of which exhibit resonances which for (B) are in all waves from $J = 0$ to $J = 4$.

Finally, a simple amplitude analysis has been made [14] which finds no compelling evidence for any resonances. However, the analysis only used data in the restricted momentum range of 360 MeV/c to 988 MeV/c and is therefore not strictly comparable with the other analyses reported here.

The work of ref. [13] is the most complete of the published analyses, but it is difficult to make a meaningful comparison with our own because of the significant difference in the input data to these two analyses i.e. our inclusion of invariant amplitudes and, via these, the requirement that the solution should be consistent with information in the $\pi N \rightarrow \pi N$ channel. To see the importance of this, we show in Fig. 3 the prediction of the solutions of ref. [13] for the invariant amplitudes as functions of t at the fixed value of $\xi = -0.04572 \text{ GeV}^2$ together with our own fit to these amplitudes. It is clear, that despite the considerable errors on the invariant amplitudes, they do provide important constraints which are not satisfied by either of the solutions of ref. [13].

Nevertheless, there are some common results found in both analyses. Both find a clear signal for the $f_4(2050)$, and both find its coupling to the $L = 3$ amplitude is much stronger than to $L = 5$. Also, both analyses yield a low-lying $J = 0$ state with a suggestion of abnormally large coupling to the $\bar{N}N$ channel. Agreement for other waves is much less good. For example, for $J = 1$ ref. [13] finds a resonance only in solution B and it couples mainly to h_{1+} , whereas the $J = 1$ resonance in our solution, although it has similar parameters, couples mainly to h_{1-} . Likewise, there are substantial differences in masses, widths and couplings for the $J = 2$ and 3 waves.

One place where it may be possible to decide between the various solutions is in the $\bar{p}p \rightarrow \pi^0\pi^0$ channel where dcs data exist for only a limited momentum range. We show in Fig. 2 our predictions together with those of ref. [13] for the differential cross section and

asymmetry in this channel at a lower momentum where there are no measurements. In the same figure we also show similar predictions at two higher momenta where measurements of the differential cross section exist [3].

In conclusion, we summarise our overall findings. We have analysed data on $\bar{p}p \rightarrow \pi\pi$, including very accurate data in the $\pi^-\pi^+$ channel, using constraints from crossing symmetry and analyticity to impose consistency of the solution with information on data in the $\pi N \rightarrow \pi N$ channel. Overall, we have found evidence for a rich spectrum of resonances whose couplings, with one or two exceptions, are in the range expected for normal daughter meson states with a $\bar{q}q$ structure. The exceptions are in low J states and have couplings far larger than expected. This may indicate the presence of more complex multi-quark structures with large couplings to the $\bar{N}N$ channel as expected in some models [15].

REFERENCES

- [1] E. Eisenhandler et al., Phys Lett. B47 536 (1973); A. Donnachie and P. R. Thomas, Nuovo Cimento 26A 317 (1975); A. A. Carter et al., Phys Lett. B67 117 (1977); B. Hyams et al., Nucl. Phys B73 202 (1974); H. Nicholson et al., Phys. Rev. D 9 2572 (1973).
- [2] E. Eisenhandler et al., Nucl. Phys B96 109 (1975); A.A. Carter et al., Nucl. Phys B127 202 (1977).
- [3] R. S. Dulude et al., Phys Lett. B79 329 (1978).
- [4] E. Barrelet, Nuovo Cimento 84 331 (1972).
- [5] A. D. Martin and M. R. Pennington, Phys Lett. B86 93 (1979); Nucl. Phys B169 216 (1980).
- [6] B. R. Martin and D. Morgan, Nucl. Phys B176 355 (1980).
- [7] B. R. Martin and D. Morgan, in *Proceedings of the IV European Antiproton Symposium, Barr, 1978*, Vol. 2, p. 101 and in *Proceedings of the V European Symposium on Nucleon-Antinucleon Interactions, Bressanone, 1980*, p. 397.
- [8] B. R. Martin and G. C. Oades, Nucl. Phys A483 669 (1988).
- [9] T. Tanimori et al., Phys. Rev. Lett. 55 1835 (1985).
- [10] B. R. Martin and G. C. Oades, in *Proceedings of the Twelfth International Conference on Particles and Nuclei, M.I.T., 1990*, edited by J. L. Mathews, T. W. Donnelly, E. H. Farhi and L. S. Osborne (North Holland, 1991), p. 496c.
- [11] A. Hassan et al., Nucl. Phys B378 3 (1992).
- [12] A. Hassan and D. V. Bugg, Phys Lett. B334 215 (1994).
- [13] M. N. Oakden and M. R. Pennington, Nucl. Phys A574 731 (1994).

[14] W. M. Kloet and F. Myhrer, Phys. Rev. D 53 6120 (1996).

[15] R. L. Jaffe, Phys. Rev. D 17 1444 (1978).

FIGURES

FIG. 1. Fits to the measured differential cross-section and asymmetry data for $\bar{p}p \rightarrow \pi^- \pi^+$. Our results are shown by solid lines and those of solution A of ref. [13] by dashed lines (solution B is very similar). (a) 404 MeV/c, (b) 1190 MeV/c, (c) 1500 MeV/c.

FIG. 2. Predictions and/or fits to the measured differential cross-section and asymmetry data for $\bar{p}p \rightarrow \pi^0 \pi^0$. Our results are shown by solid lines and those of ref. [13] by dashed lines. (a) 404 MeV/c, (b) 1190 MeV/c, (c) 1500 MeV/c.

FIG. 3. Fits to the real and imaginary parts of B^\pm and C^\pm as functions of t at a fixed value of the hyperbolic parameter $\xi = -0.04572 \text{ GeV}^2$. The range of values for a given value of t from ref. [8] are shown by the vertical lines, our fits are shown by solid lines and the predictions of ref. [13] by dashed lines. All values are in GeV units. (a) $C^{(+)}$, (b) $B^{(+)}$, (c) $C^{(-)}$, (d) $B^{(-)}$.

FIG. 4. Results of fitting the JL basis partial wave helicity amplitudes as functions of energy with parametric forms incorporating partial-wave analyticity based on eq.11 shown by the solid lines, and with simple resonance plus background forms, eq.17, shown by the dashed lines. The solid circles show the results of the single energy analyses. (a) $J = 0, L = 1$, (b) $J = 1, L = 0$, (c) $J = 1, L = 2$, (d) $J = 2, L = 1$, (e) $J = 2, L = 3$, (f) $J = 3, L = 2$, (g) $J = 3, L = 4$, (h) $J = 4, L = 3$, (i) $J = 4, L = 5$, (j) $J = 5, L = 4$, (k) $J = 5, L = 6$.

TABLES

TABLE I. Values of χ^2 per data point obtained in fits to differential cross-section and asymmetry data for $\bar{p}p \rightarrow \pi^- \pi^+$, differential cross-section data for $\bar{p}p \rightarrow \pi^0 \pi^0$ and amplitude data

Momentum (MeV/c)	$\pi^- \pi^+$	$\pi^0 \pi^0$	Amplitudes
360	1.89		0.03
404	1.29		0.03
467	1.76		0.05
497	2.32		0.04
523	1.68		0.05
585	1.96		0.05
679	1.70		0.04
783	1.49		0.03
886	1.05		0.03
988	1.40		0.07
1089	1.40		0.10
1190	1.64	0.28	0.09
1291	1.76	0.66	0.15
1351	2.16	0.12	0.22
1400	1.91	0.18	0.18
1416	1.69	0.36	0.17
1449	1.80	0.23	0.26
1467	1.75	0.20	0.31
1500	1.46	0.41	0.38
1550	1.66	0.35	0.35

TABLE II. Resonance masses and widths in units of GeV, obtained from fitting partial-wave amplitudes as functions of energy, together with the values of the product of branching ratios $B_J \equiv B(R \rightarrow \pi\pi)B(R \rightarrow \bar{N}N)$.

J	Mass	Width	B_J
0	1.94, 1.95	0.16	0.18, 0.19
1	1.96, 1.97	0.13, 0.14	0.053, 0.056
2	1.93	0.15	0.013
3	2.02	0.26, 0.22	0.013, 0.028
4	2.02, 2.00	0.26, 0.14	0.013, 0.004
5	2.19	0.22	0.004, 0.001

Figure 1(a)

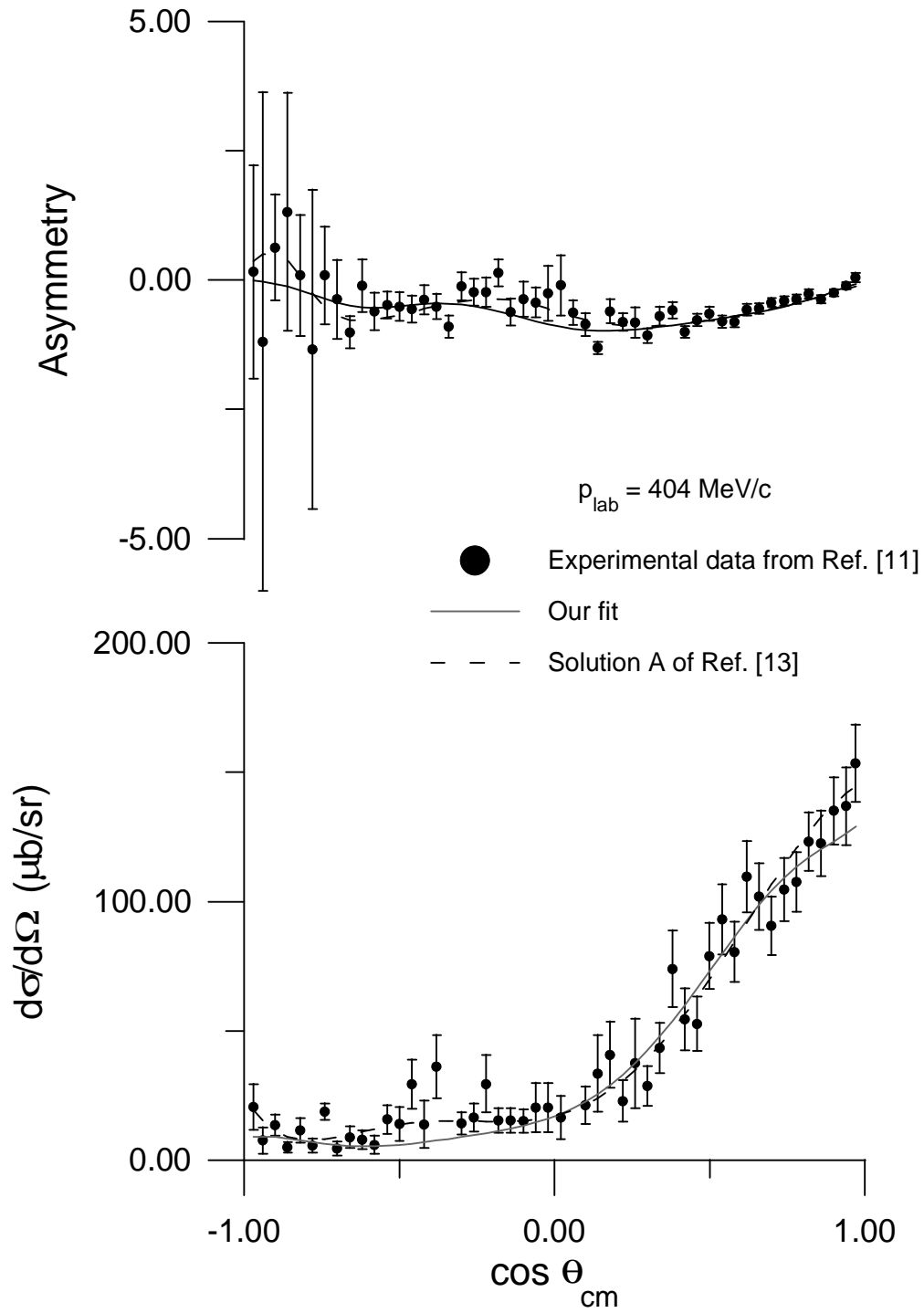


Figure 1(b)

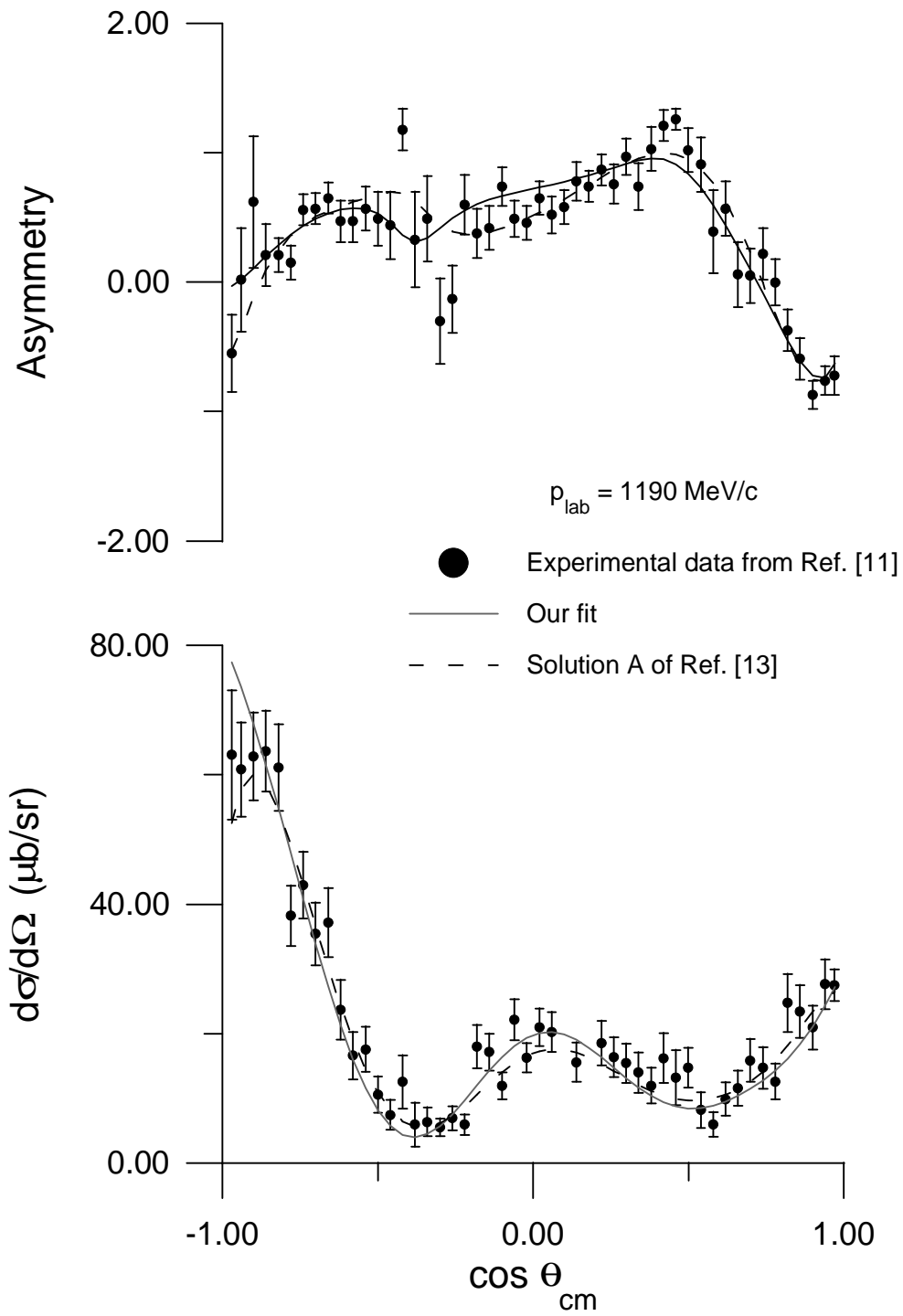


Figure 1(c)

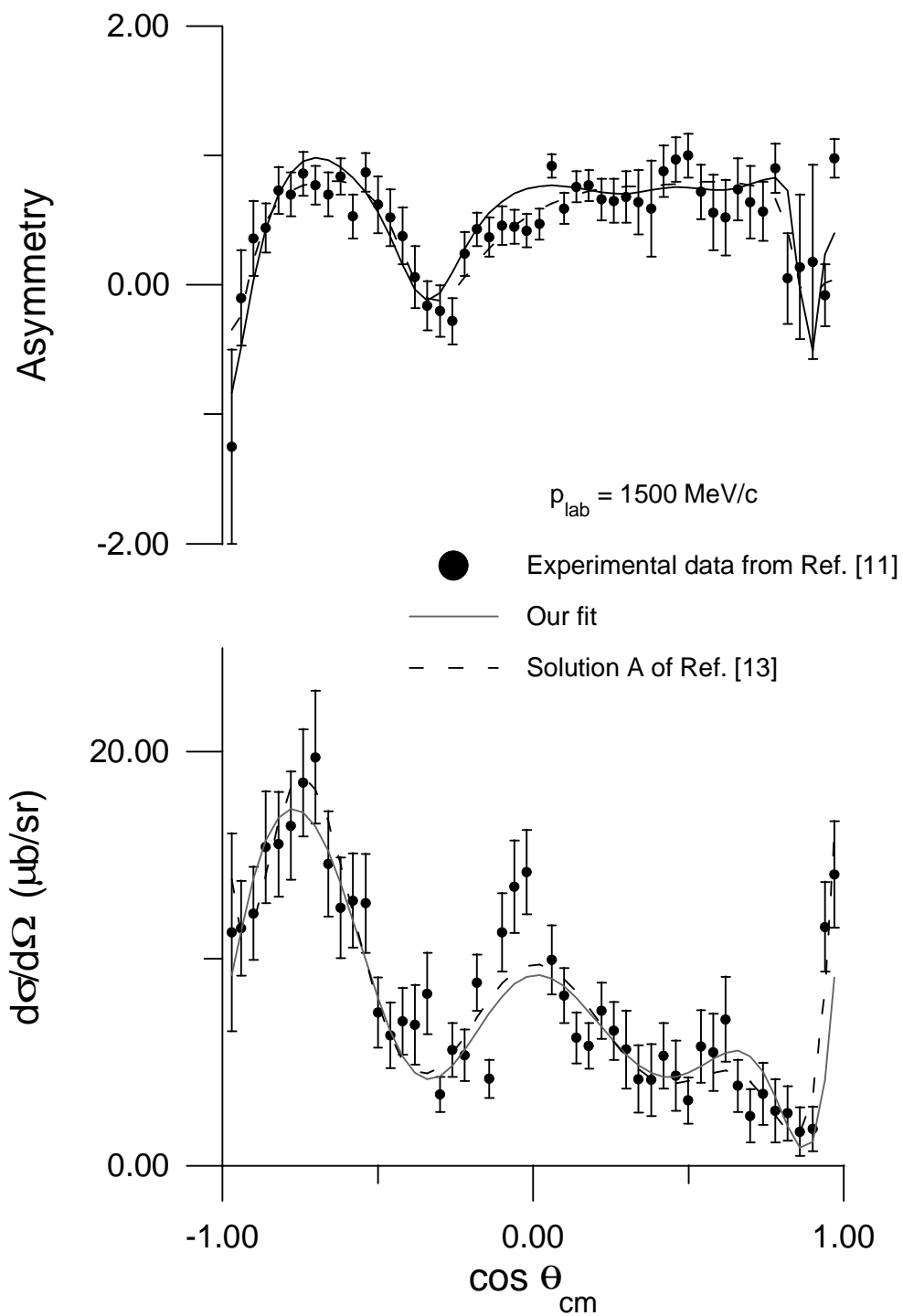


Figure 2(a)

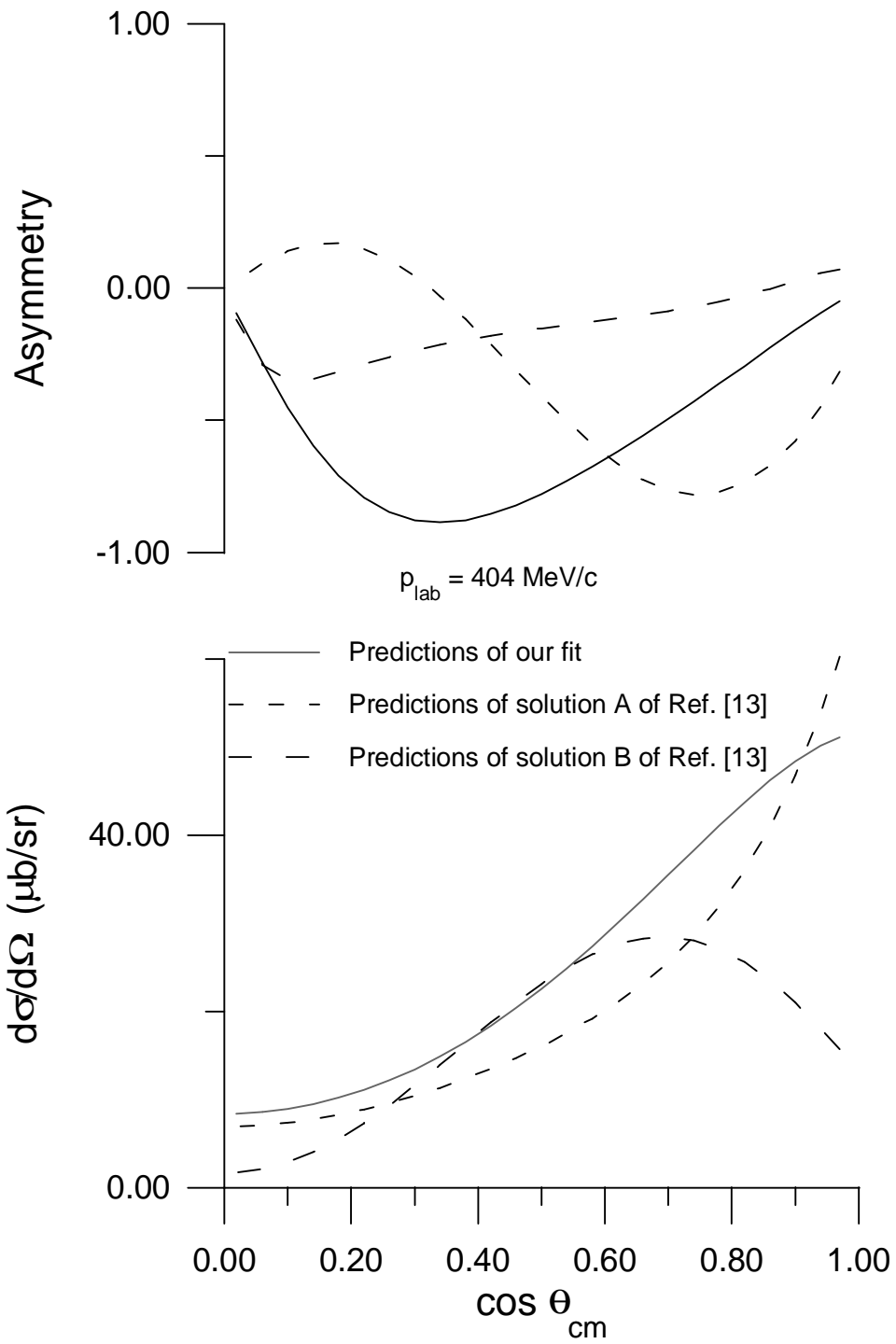


Figure 2(b)

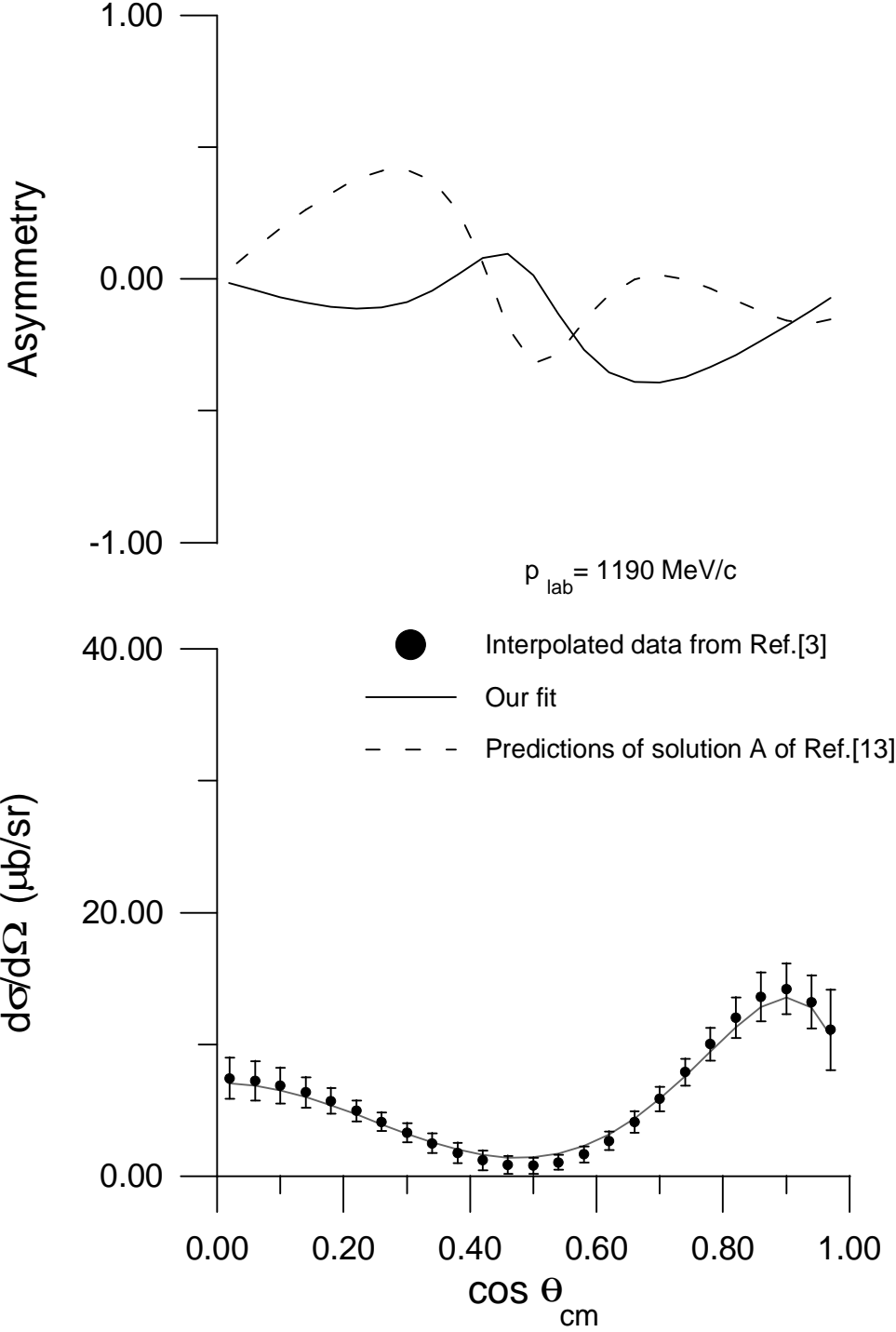


Figure 2(c)

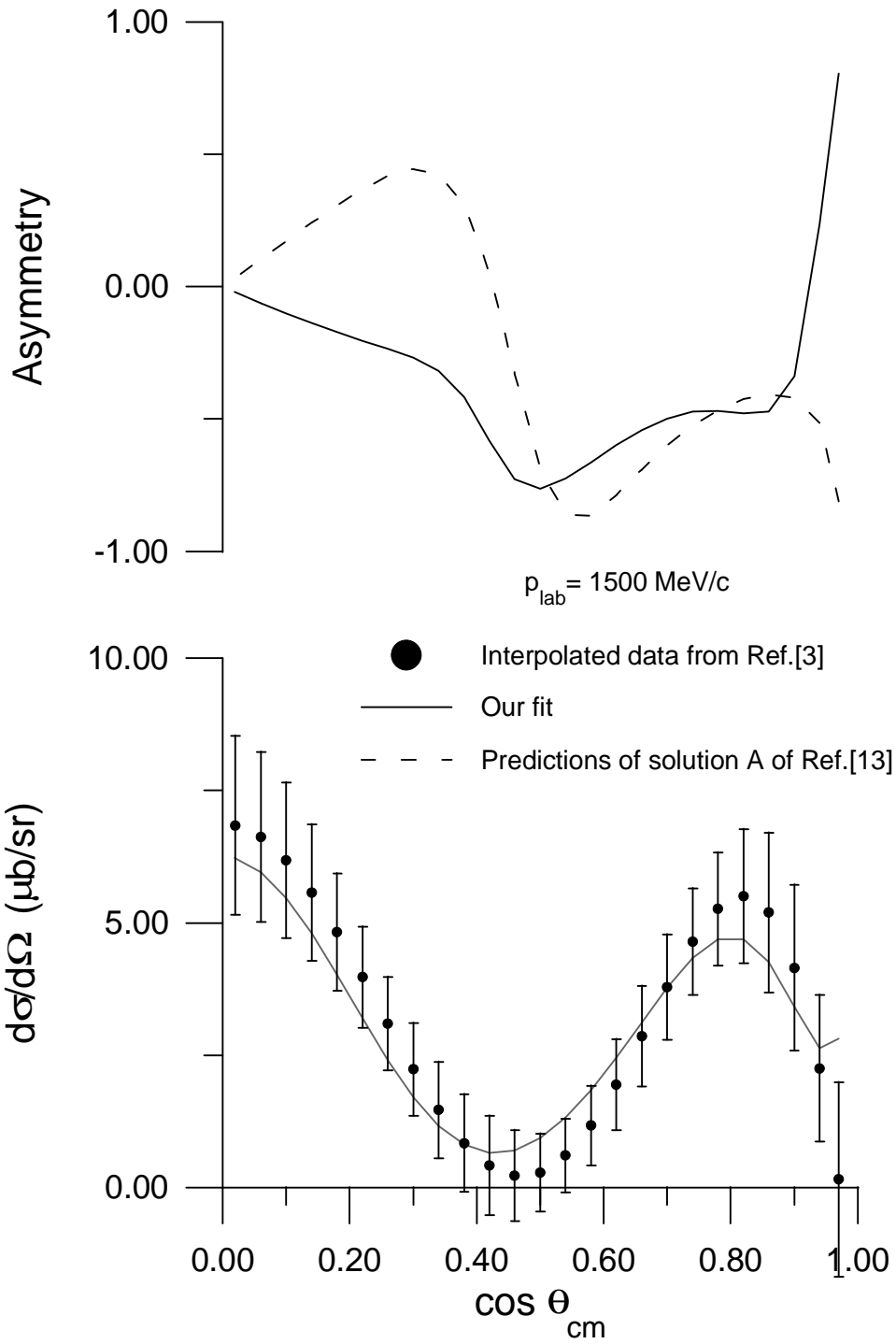


Figure 3(a)

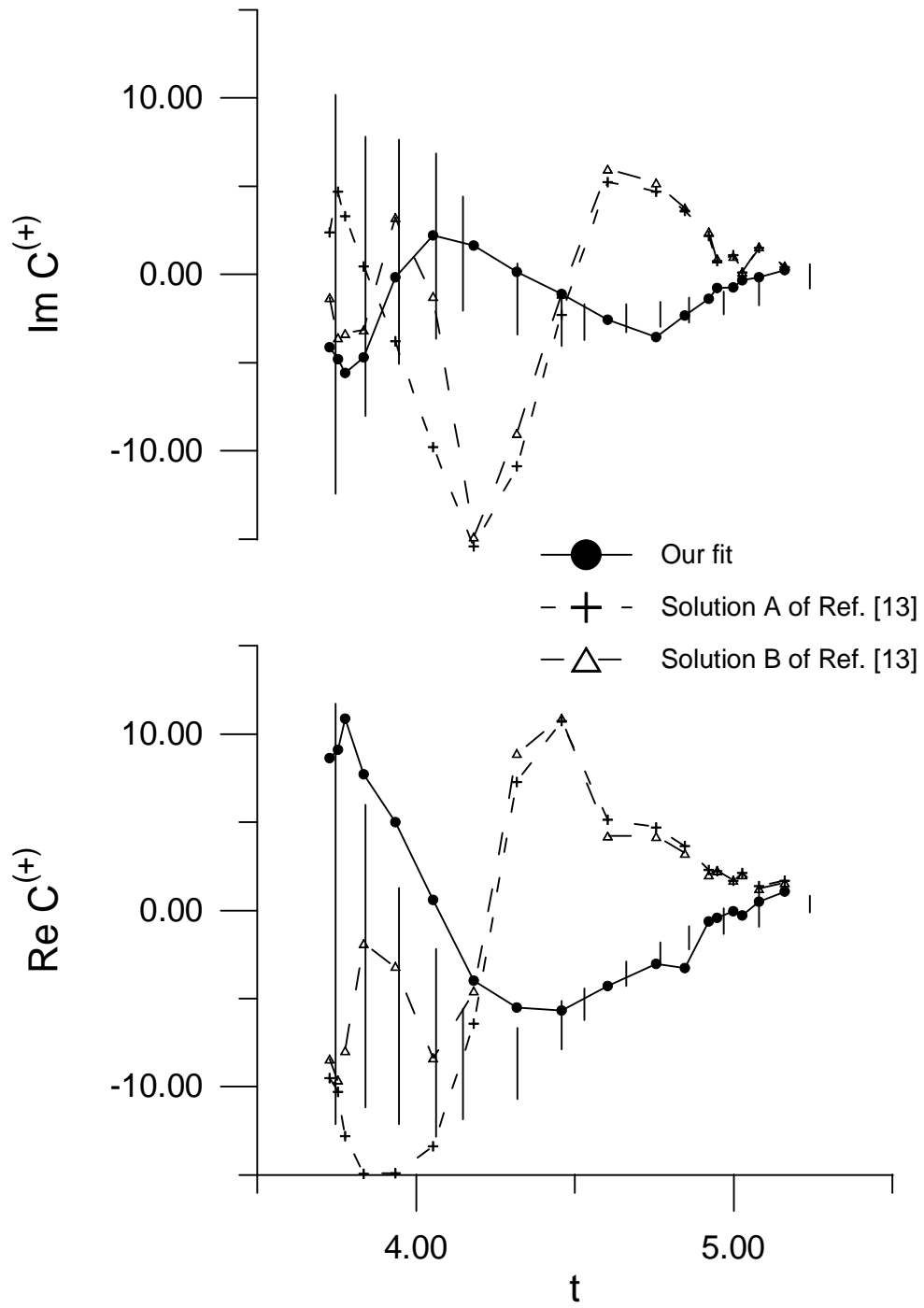


Figure 3(b)

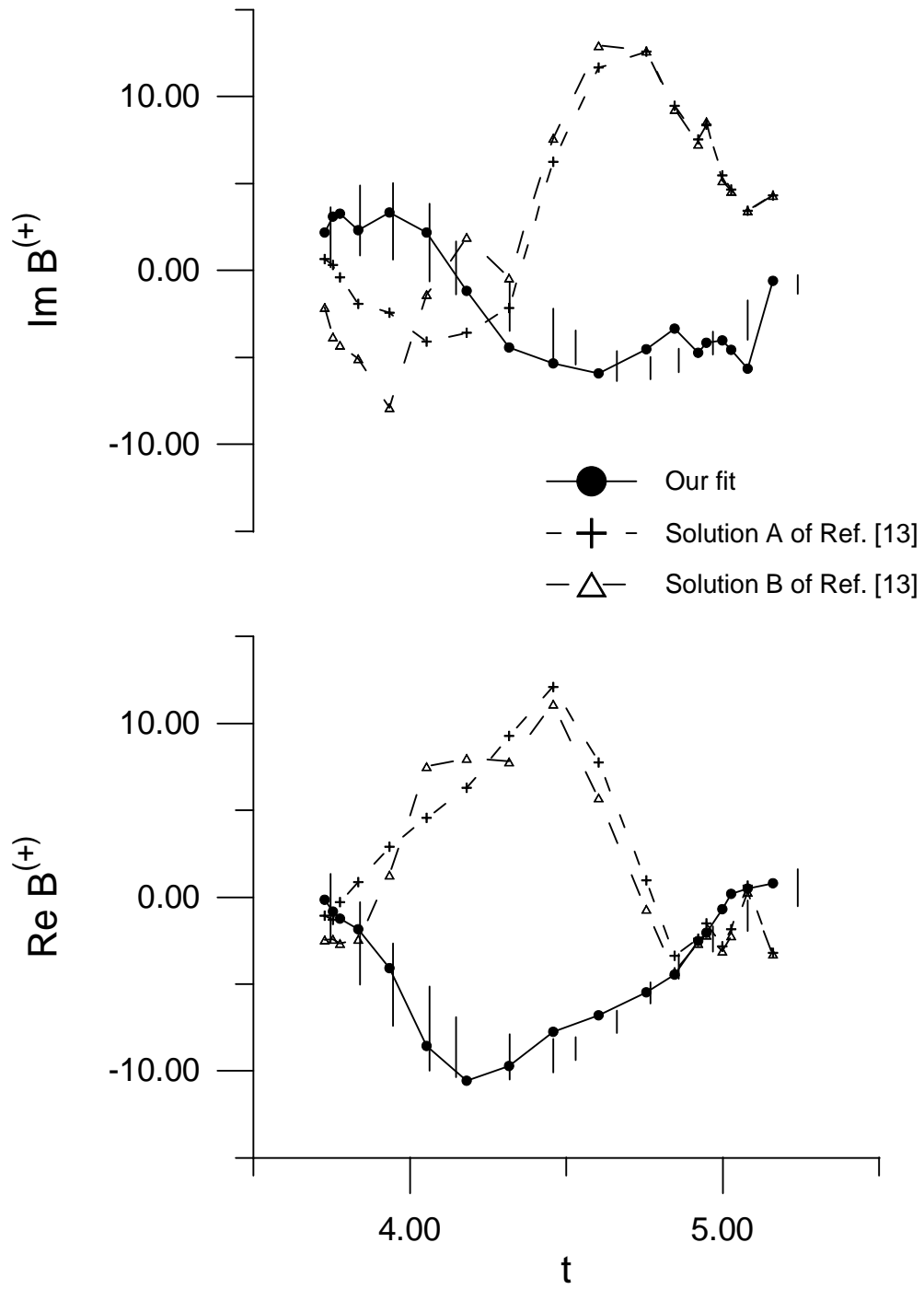


Figure 3(c)

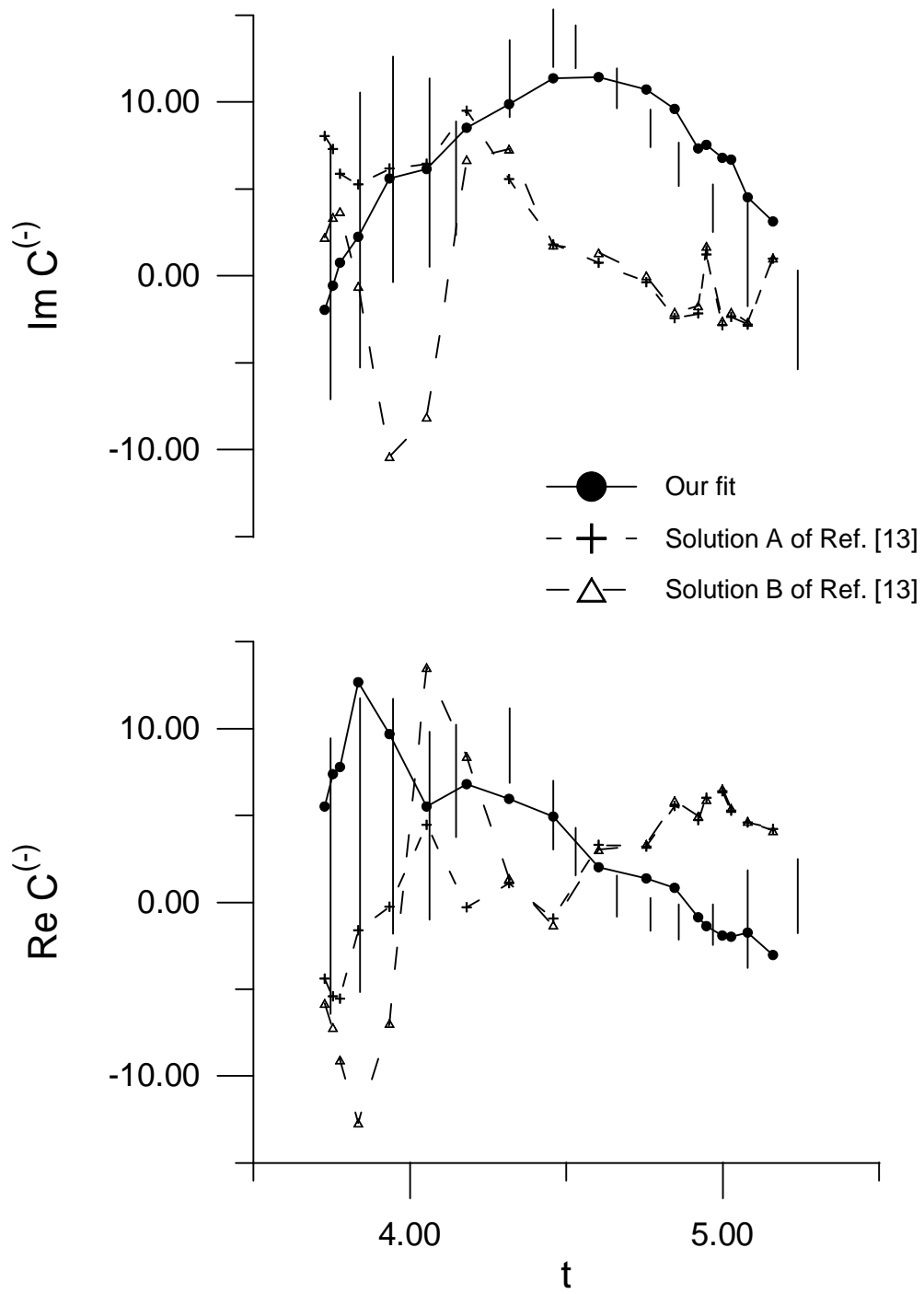


Figure 3(d)

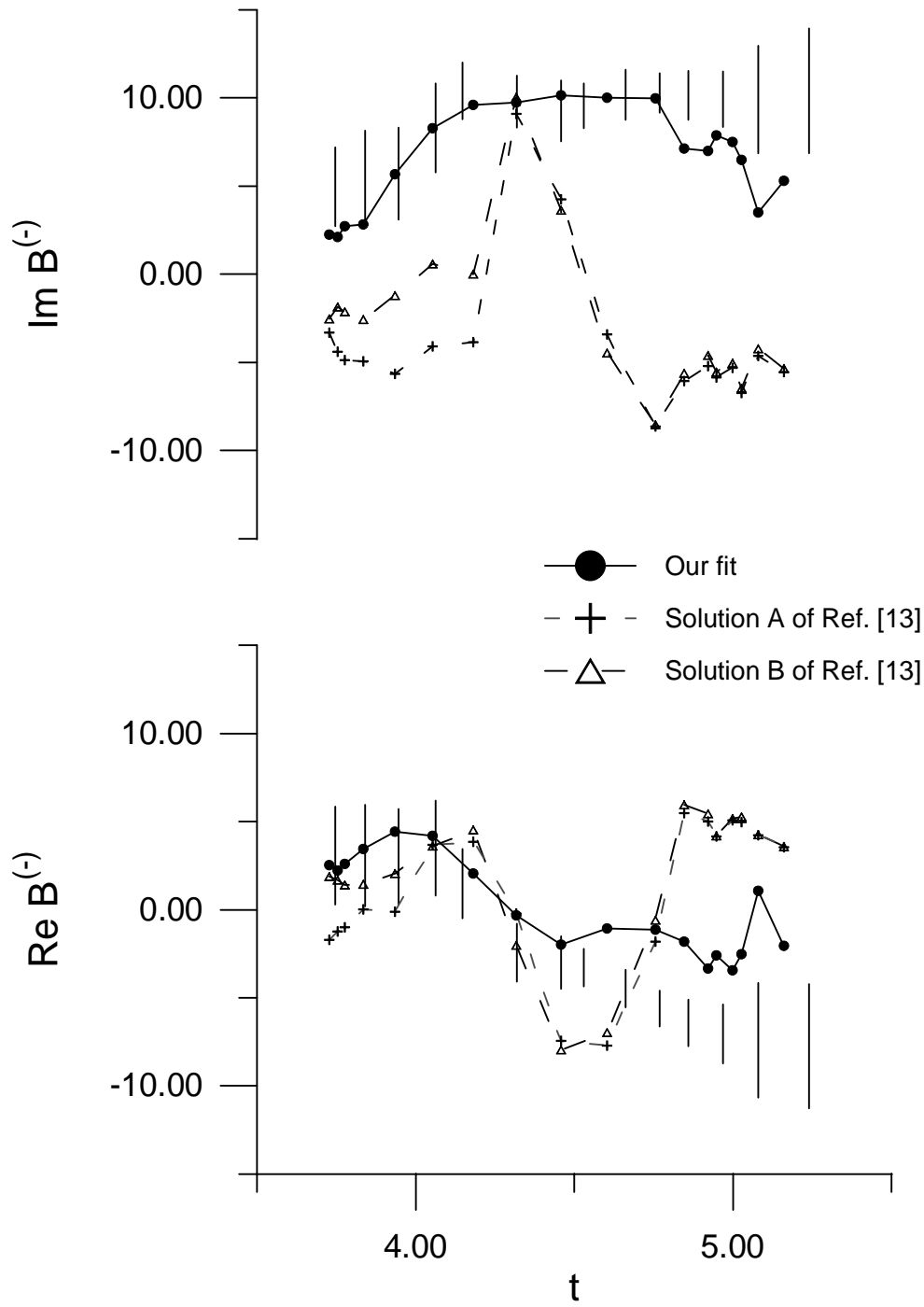


Figure 4(a)

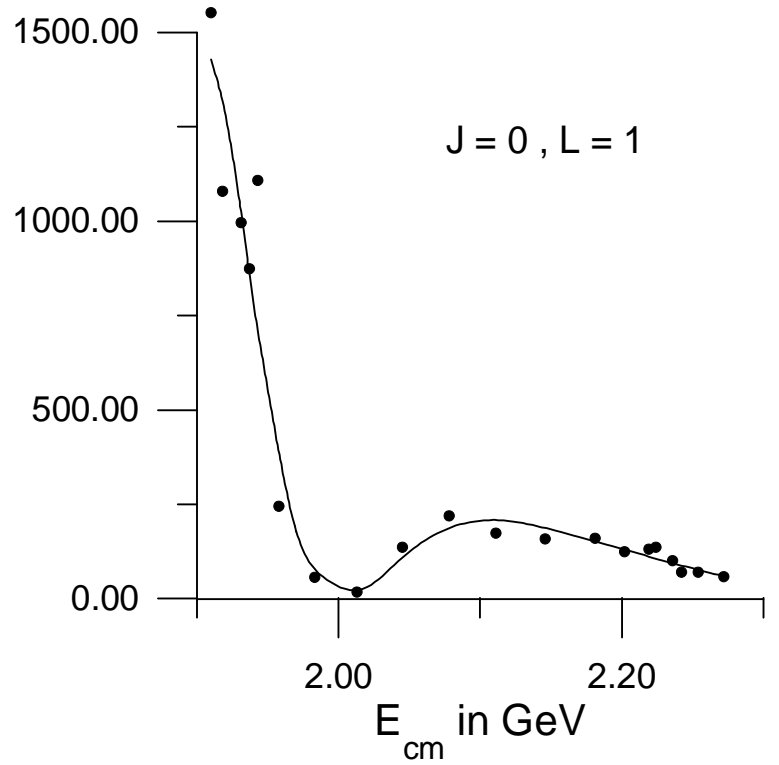
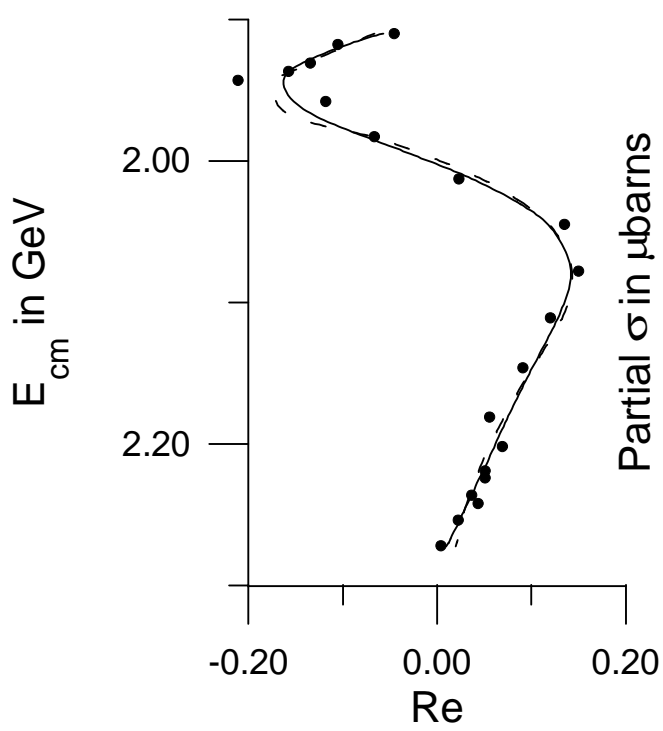
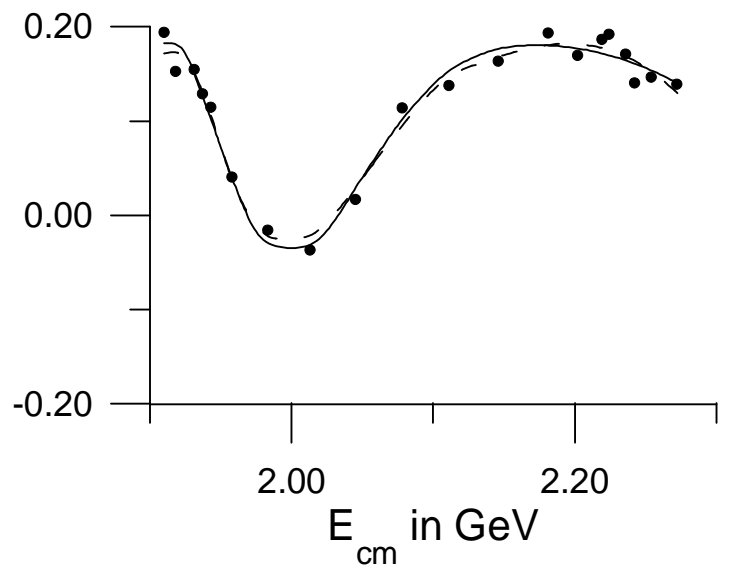
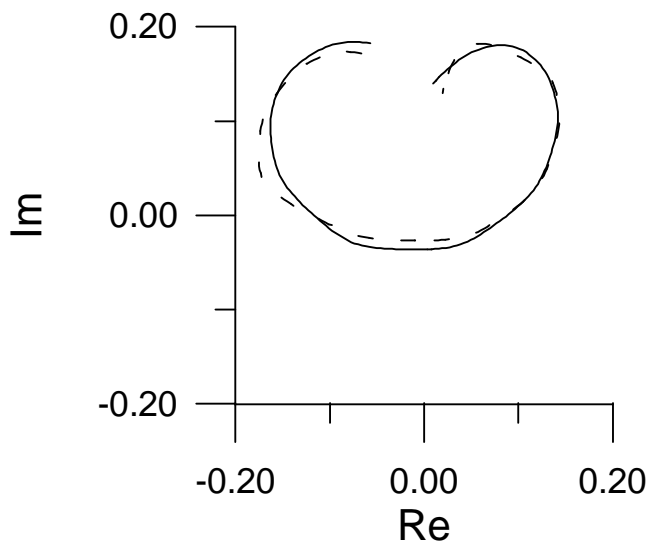


Figure 4(b)

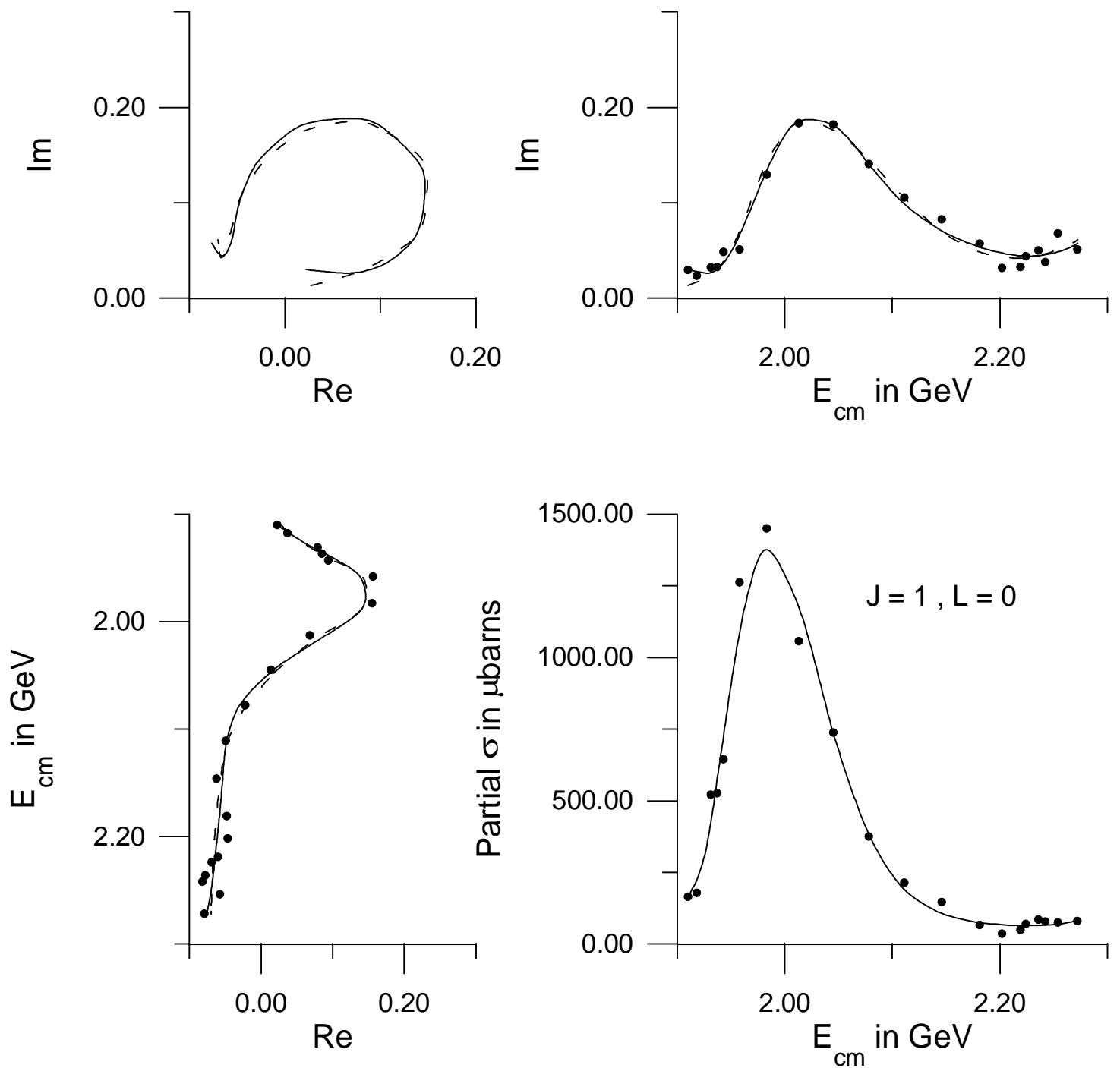


Figure 4(c)

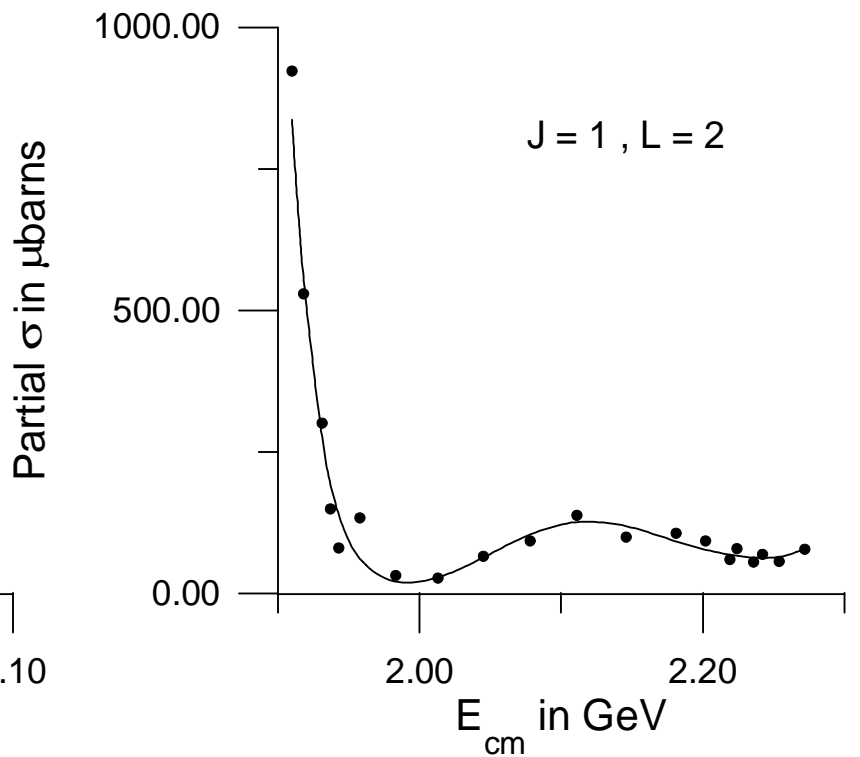
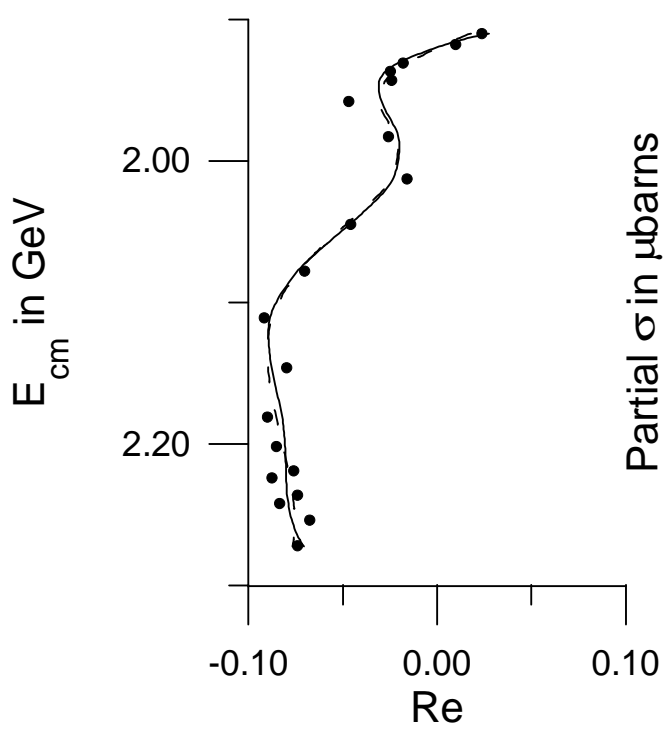
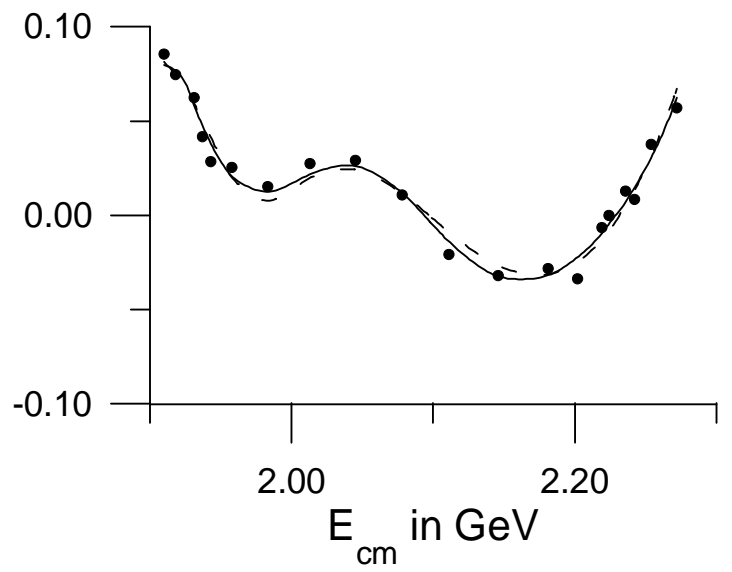
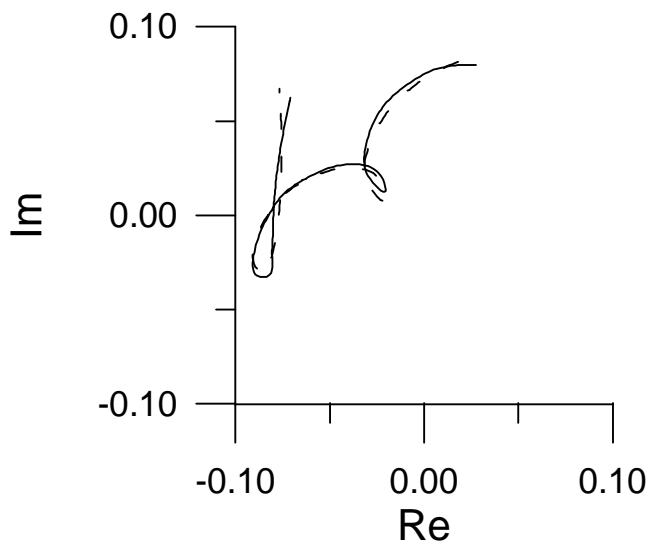


Figure 4(d)

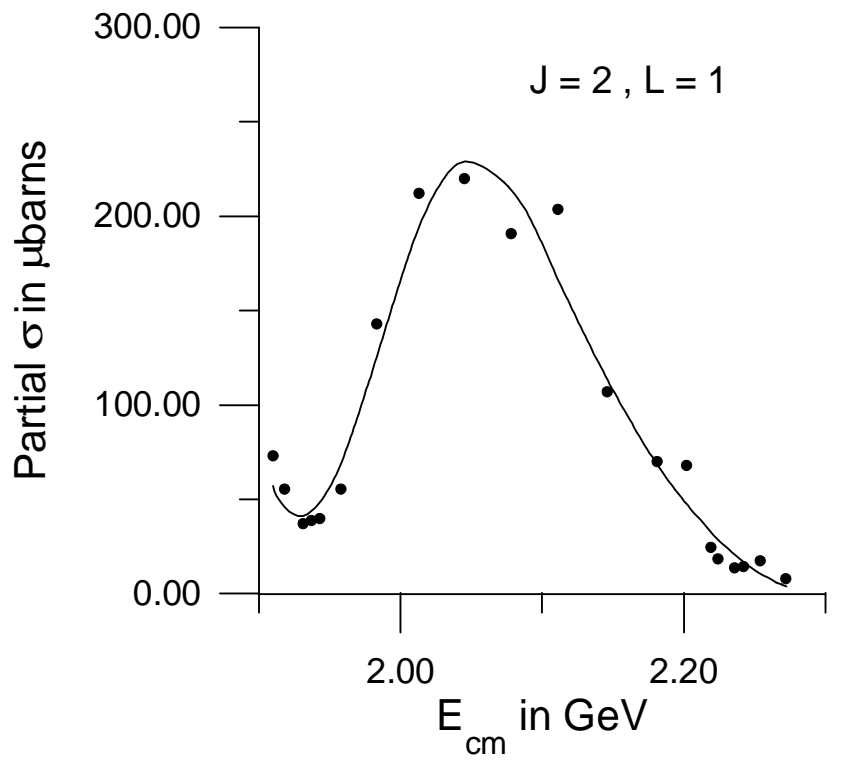
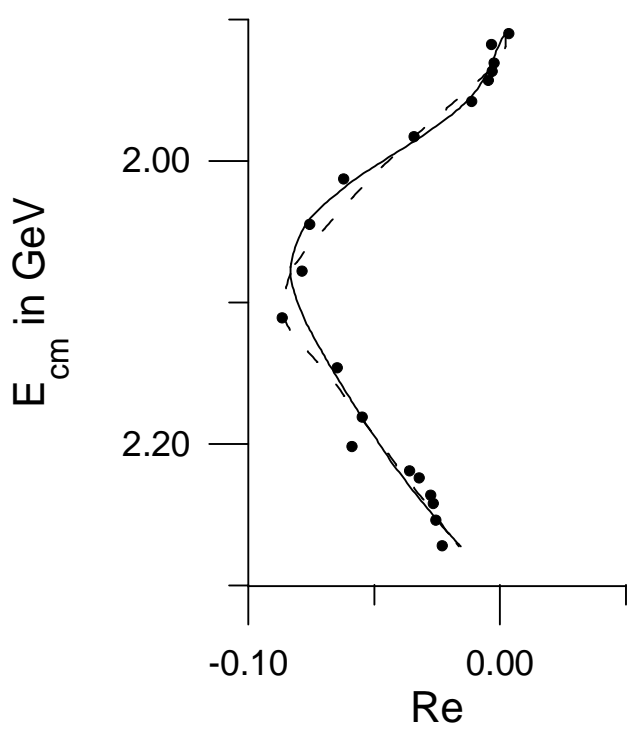
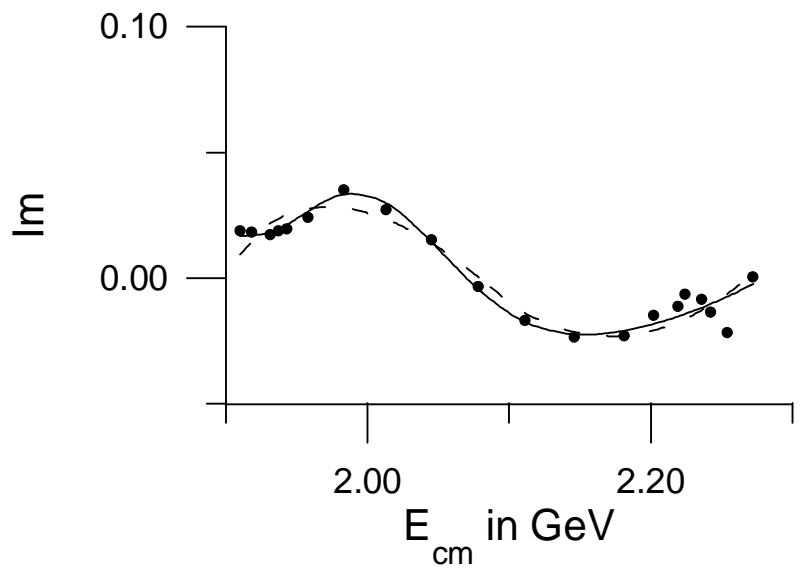
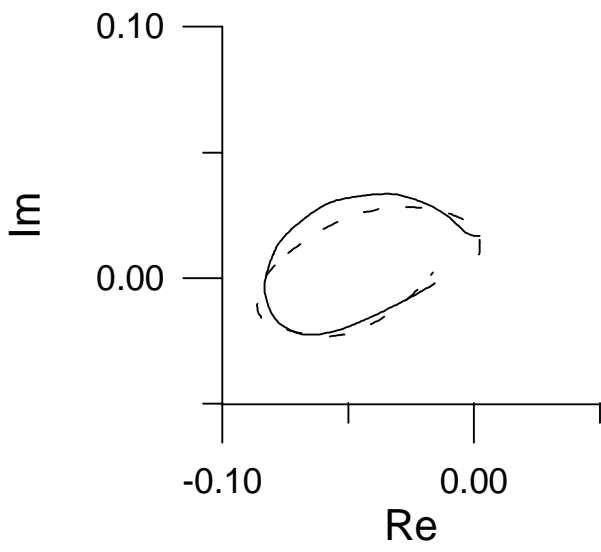


Figure 4(e)

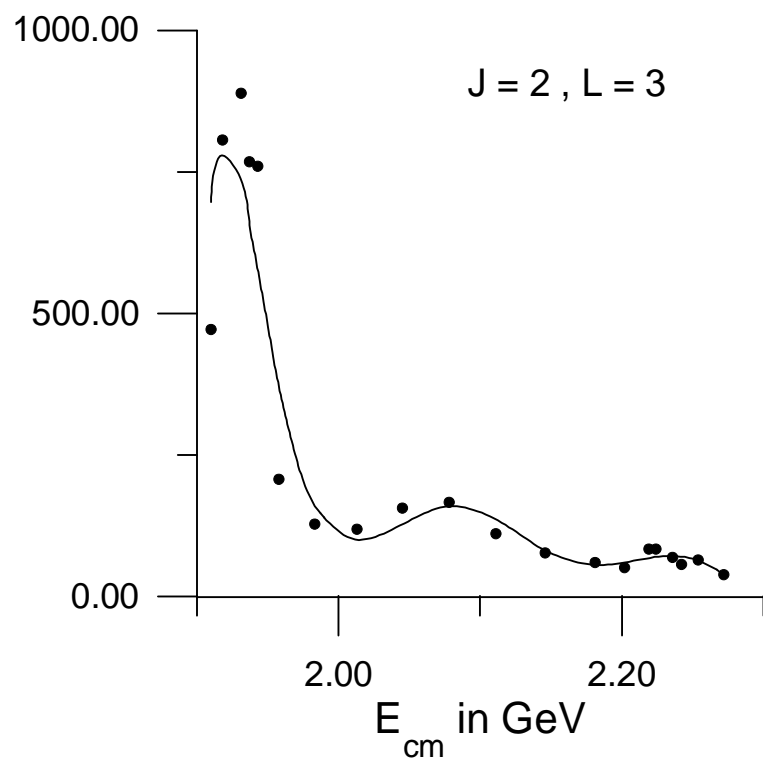
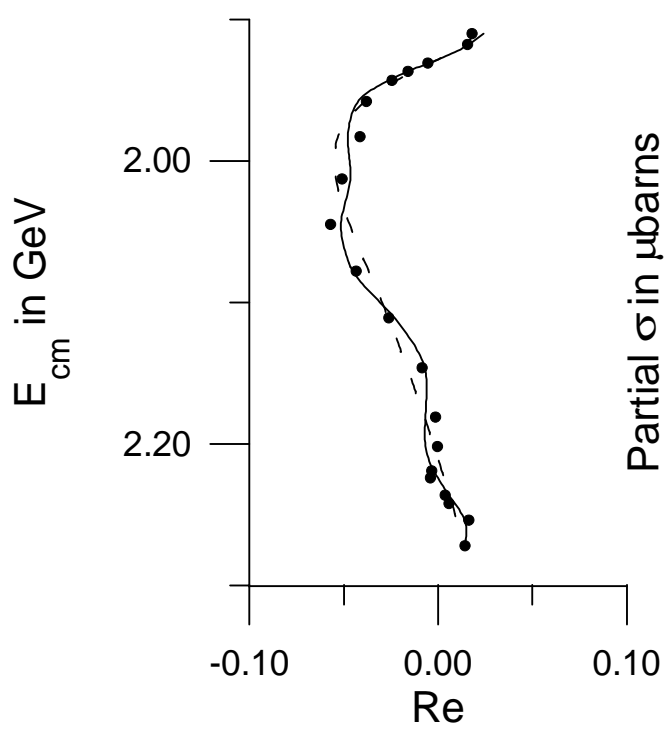
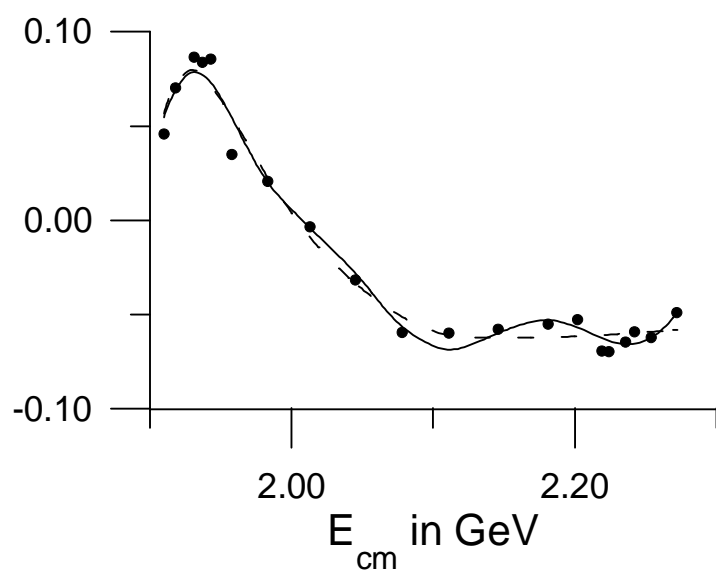
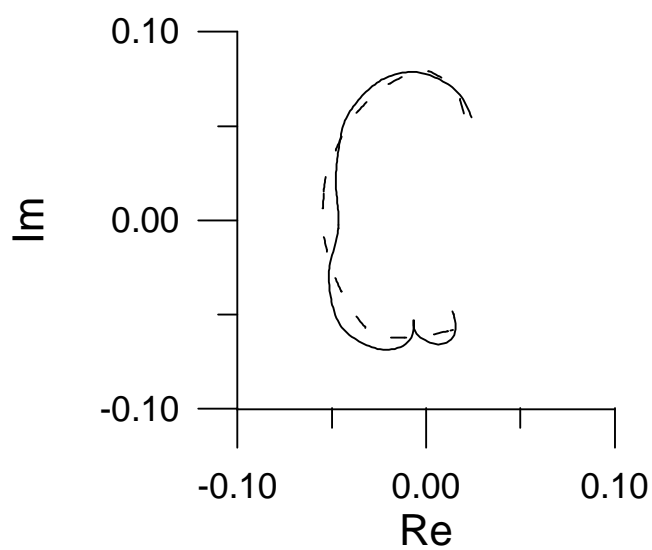


Figure 4(f)

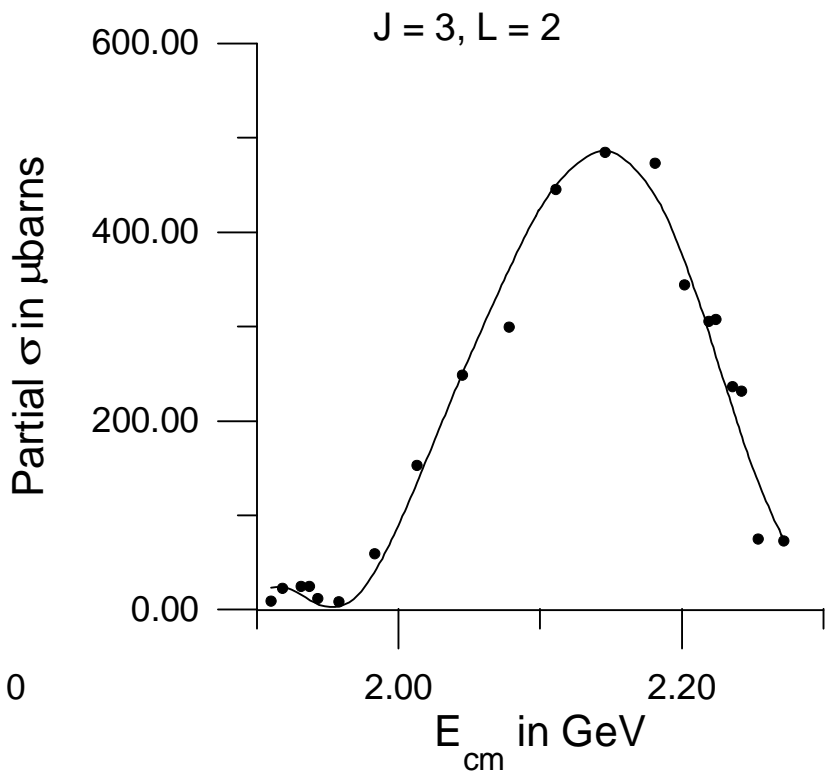
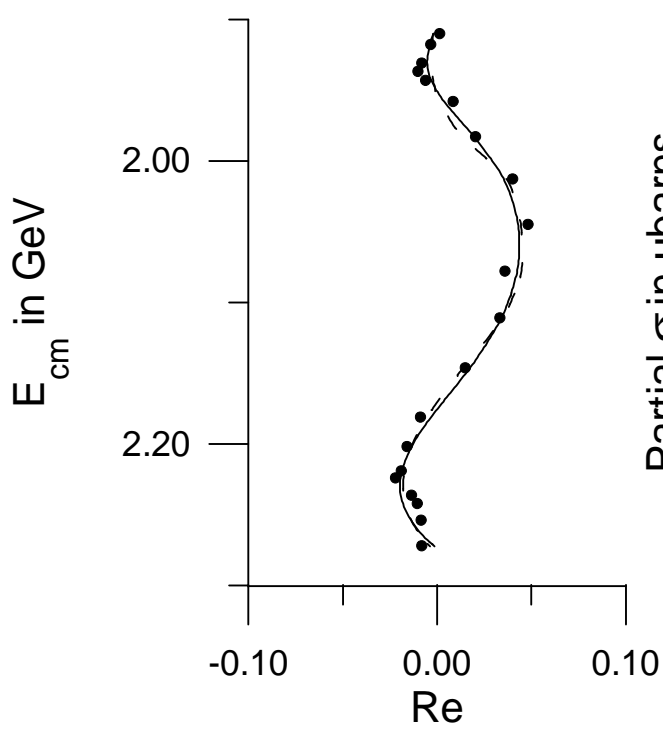
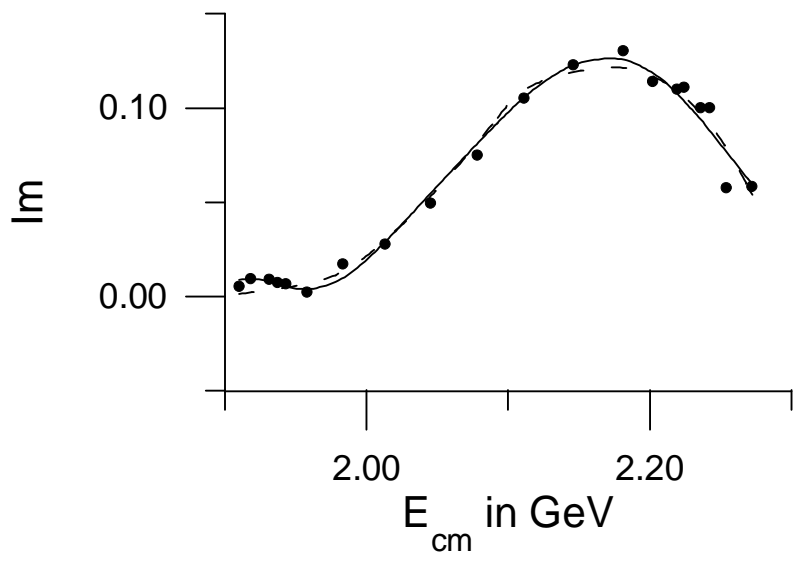
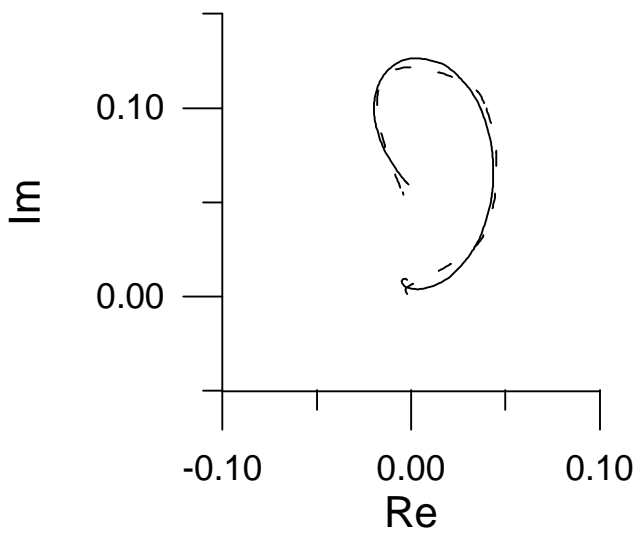


Figure 4(g)

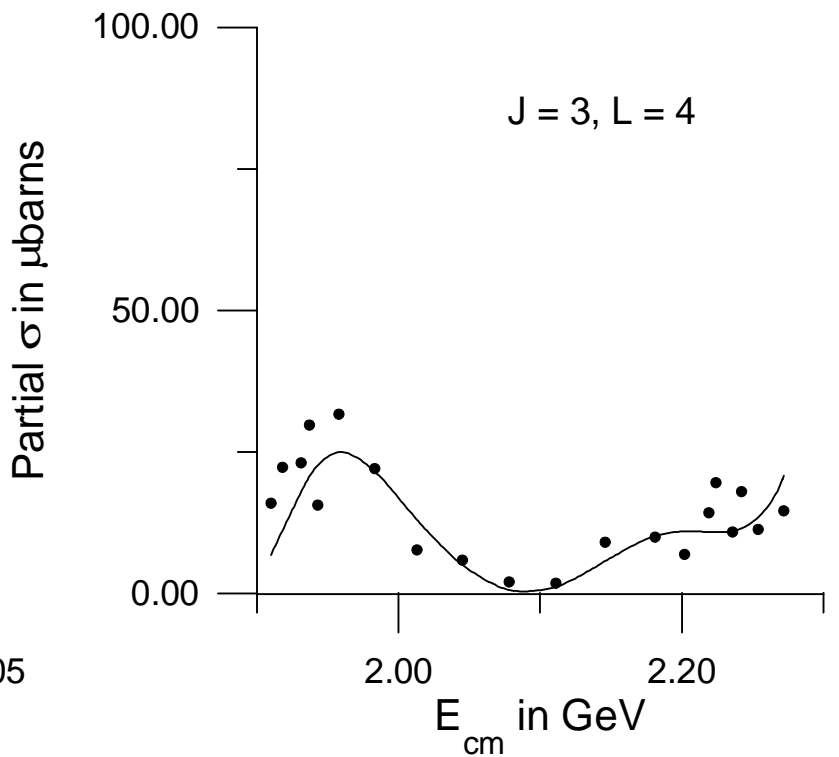
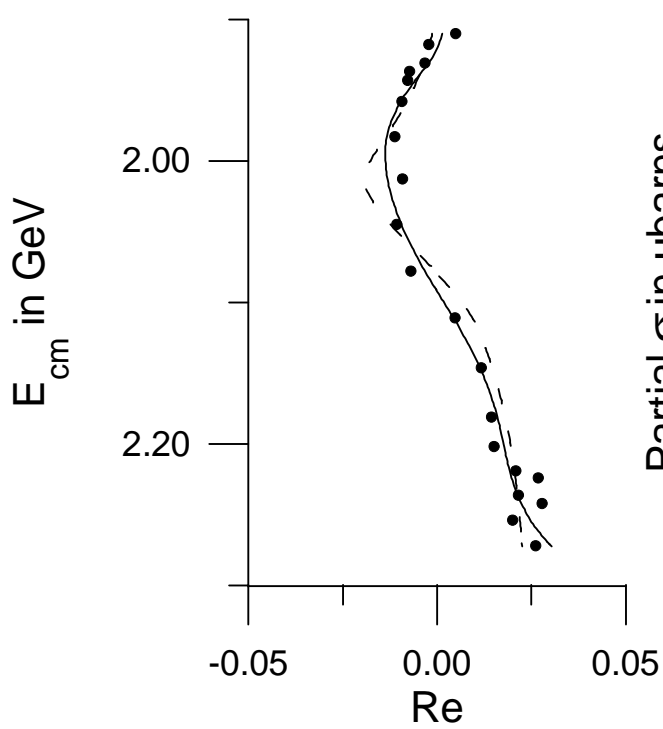
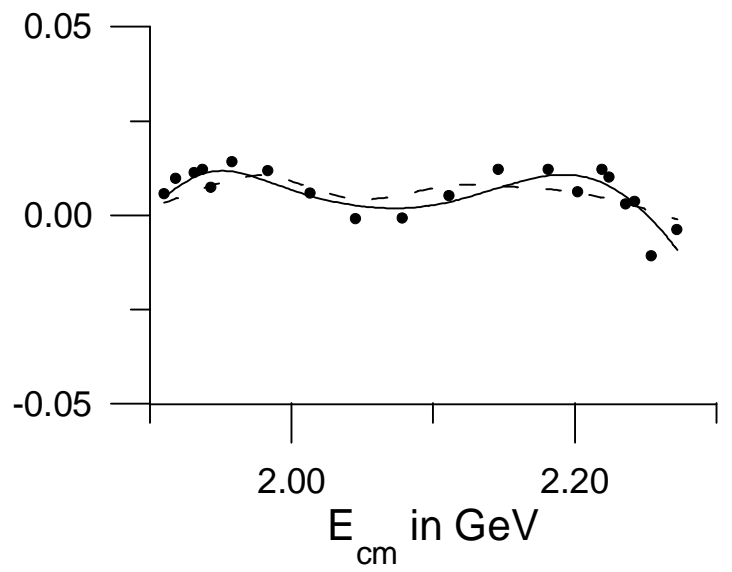
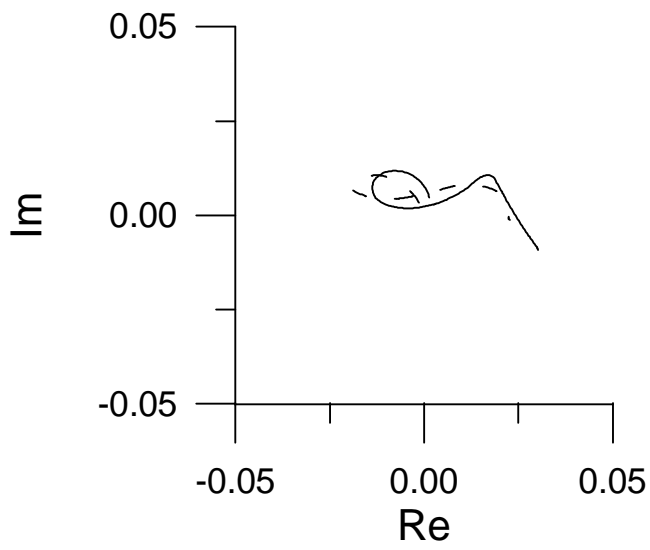


Figure 4(h)

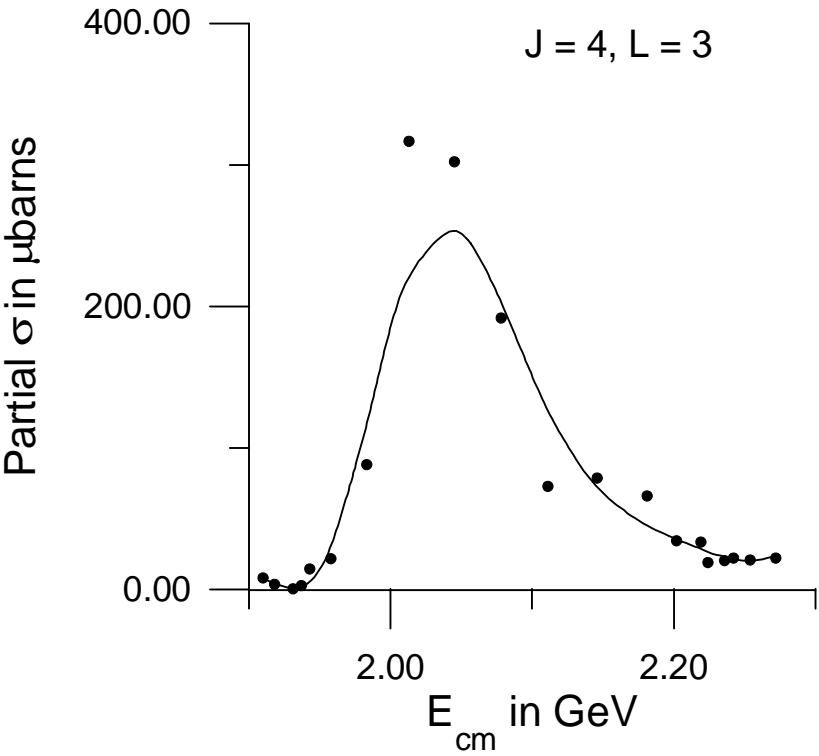
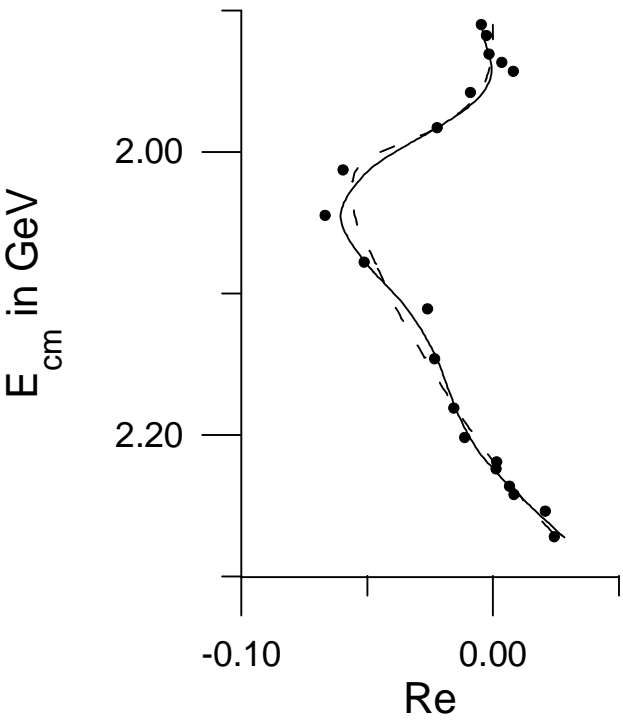
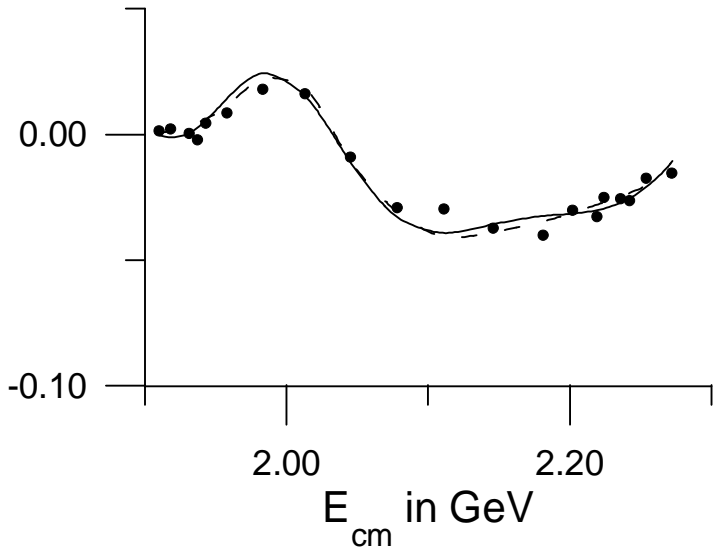
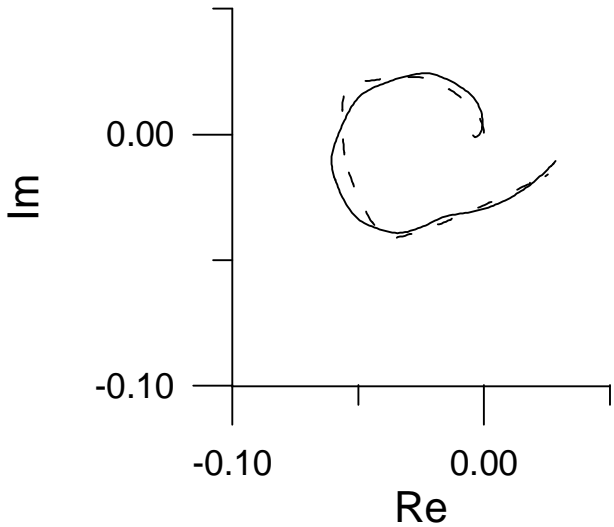


Figure 4(i)

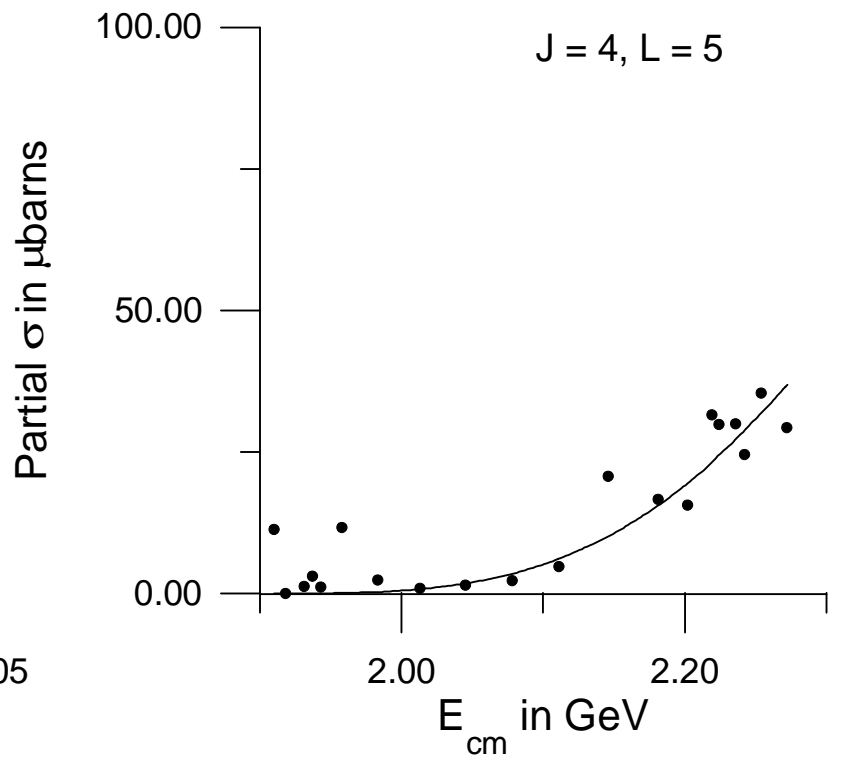
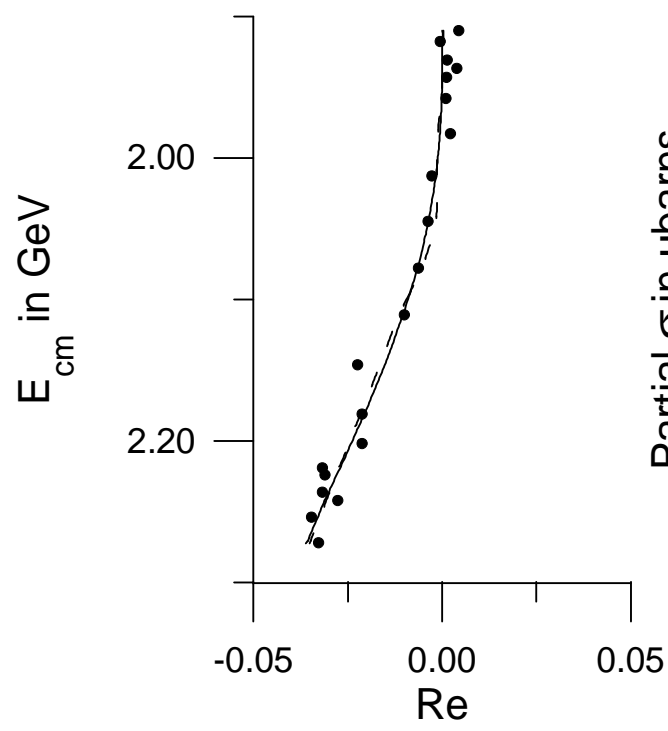
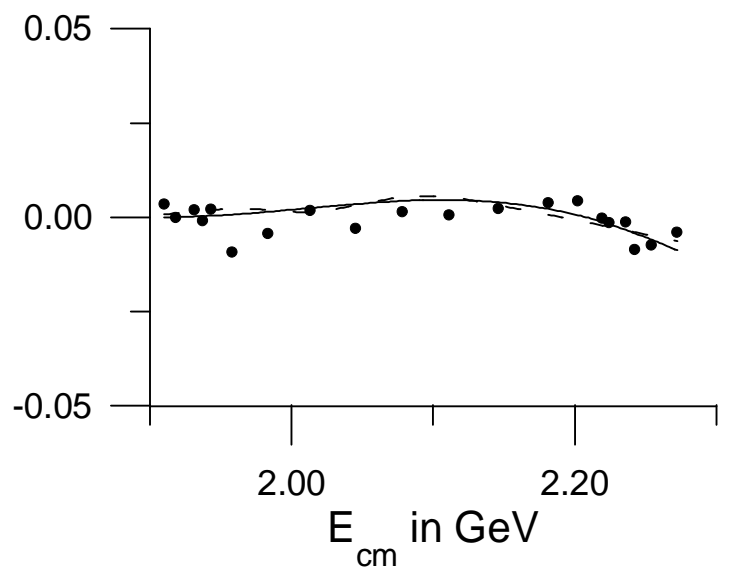
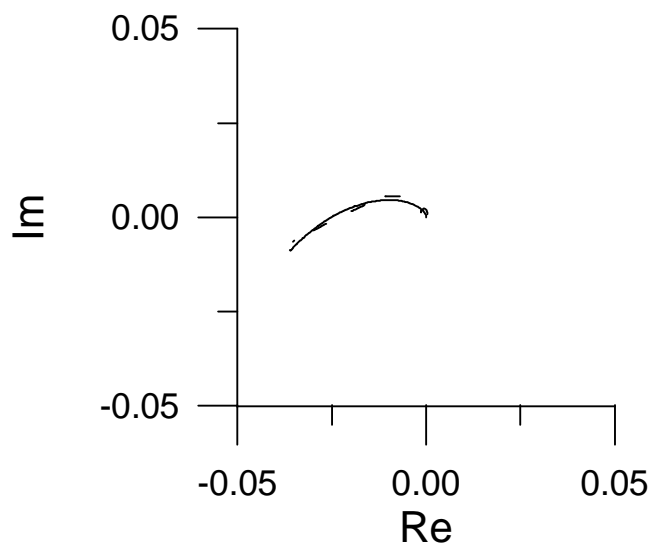


Figure 4(j)

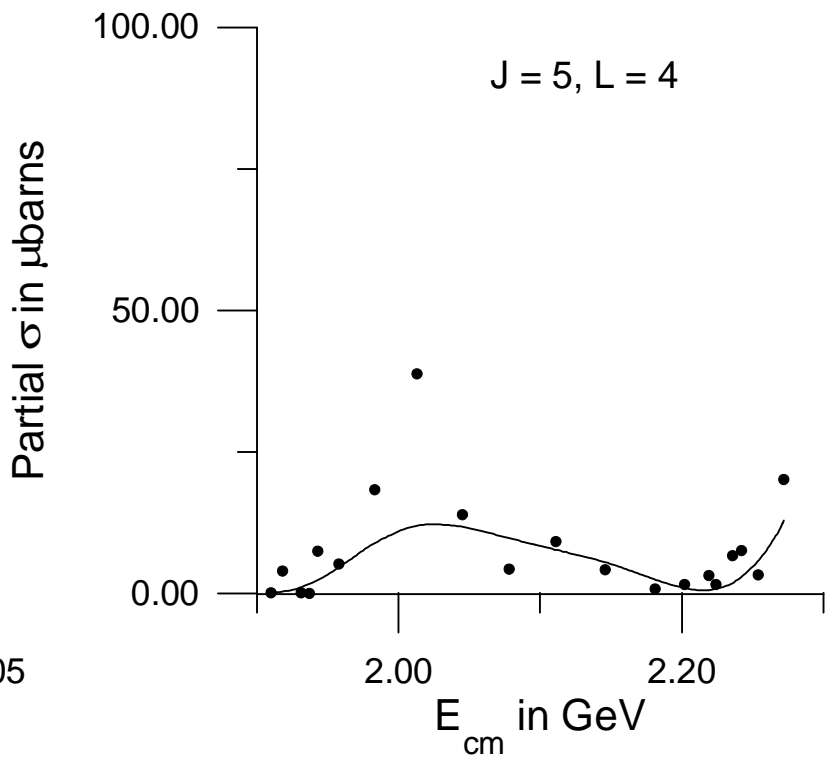
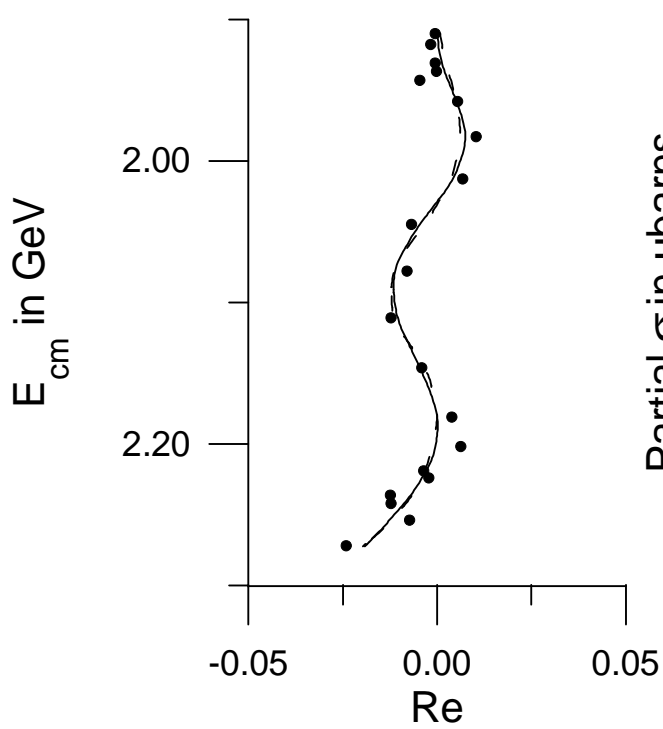
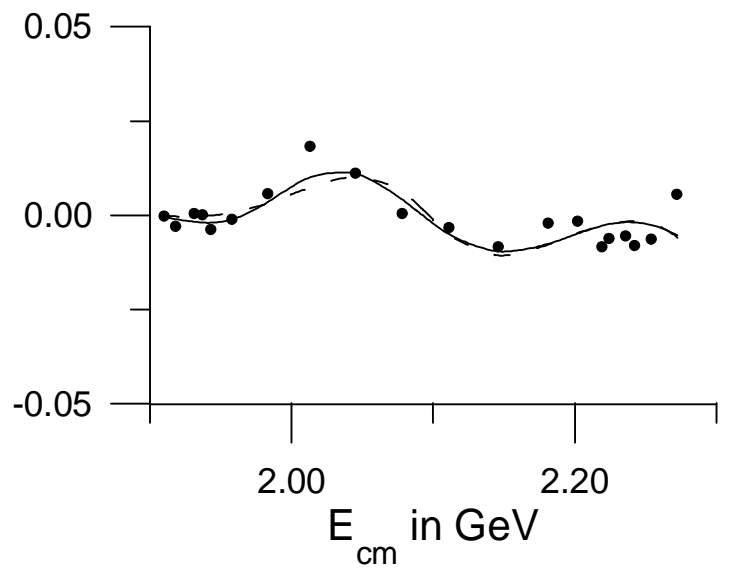
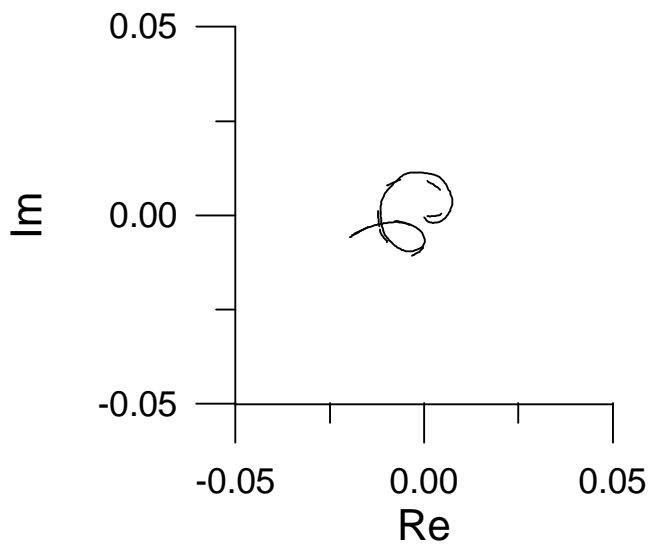


Figure 4(k)

